Astronomy & Astrophysics manuscript no. July 21, 2004
(DOI: will be inserted by hand later)

Restframe *I*-band Hubble diagram for type Ia supernovae up to $z \sim 0.5$

S. Nobili[1,2], R. Amanullah[1], G. Garavini[1,2], A. Goobar[1], C. Lidman[3], V. Stanishev[1], G. Aldering[4], P. Antilogus[2], P. Astier[2], M. S. Burns[5], A. Conley[4,6], S. E. Deustua[7], R. Ellis[8], S. Fabbro[9], V. Fadeyev[4], G. Folatelli[1], R. Gibbons[4], G. Goldhaber[4,6], D. E. Groom[4], I. Hook[10], D. A. Howell[4], A. G. Kim[4], R. A. Knop[11], P. E. Nugent[4], R. Pain[2], S. Perlmutter[4], R. Quimby[4], J. Raux[2], N. Regnault[4], P. Ruiz-Lapuente[12], G. Sainton[2], K. Schahmaneche[2], E. Smith[11], A. L. Spadafora[4], L. Wang[4], and
(THE SUPERNOVA COSMOLOGY PROJECT)

[1] Department of Physics, Stockholm University, Albanova University Center, S-106 91 Stockholm, Sweden
[2] LPNHE, CNRS-IN2P3, University of Paris VI & VII, Paris, France
[3] European Southern Observatory, Alonso de Cordova 3107, Vitacura, Casilla 19001, Santiago 19, Chile
[4] E. O. Lawrence Berkeley National Laboratory, 1 Cyclotron Rd., Berkeley, CA 94720, USA
[5] Colorado College, 14 East Cache La Poudre St., Colorado Springs, CO 80903
[6] Department of Physics, University of California Berkeley, Berkeley, 94720-7300 CA, USA
[7] American Astronomical Society, 2000 Florida Ave, NW, Suite 400, Washington, DC, 20009 USA
[8] California Institute of Technology, E. California Blvd, Pasadena, CA 91125, USA
[9] CENTRA-Centro M. de Astrofísica and Department of Physics, IST, Lisbon, Portugal
[10] Department of Physics, University of Oxford, Nuclear & Astrophysics Laboratory, Keble Road, Oxford, OX1 3RH, UK
[11] Department of Physics and Astronomy, Vanderbilt University, Nashville, TN 37240, USA
[12] Department of Astronomy, University of Barcelona, Barcelona, Spain

Add footnote number "6" to Perlmutter (I'm now also in the physics department).

Received ...; accepted ...

Abstract. Using a novel technique for fitting restframe *I*-band lightcurves of type Ia supernovae, a Hubble diagram including 26 SNe with $0.01 < z < 0.1$ was constructed. Adding three SNe at $z \sim 0.5$ yields results that support the expectations for a flat Λ-dominated "concordance universe" $(\Omega_M, \Omega_\Lambda)=(0.3,0.7)$. The high redshift supernova NIR data was also used to test for systematic effects in the use of SNIa as distance estimators. A flat, $\Lambda = 0$, universe where the faintness of supernovae at $z \sim 0.5$ is due to gray dust homogeneously distributed in the intergalactic medium is disfavored based on the high-z Hubble diagram using this preliminary data-set. However, the uncertainties are large and no firm conclusion may be drawn. We also show that more supernovae are necessary to set limits on intergalactic dust based on $B-I$ and $B-V$ color measurements. The high redshift restframe *I*-band lightcurves are better fit by templates that s peak, suggesting that they are not intrinsically subluminous.

Key words. cosmology:observations, supernovae: general

Isn't our best concordance universe Omega_M = 0.25, Omega_Lambda = 0.75 (see Knop et al)? We need some way to easily handle this small difference throughout this paper. Perhaps one or two places where we show that it doesn't make any difference. And also we should make the "=" signs "approximately equal" signs in these two sentences.

best fit by a cosmological model that includes

at redshifts of z ~ 0.5

1. Introduction

Observations of type Ia supernovae (SNe) in restframe *B*-band up to $z \sim 1$ and above have shown that they are significantly dimmer than expected in a universe without a cosmological constant or some other form of dark energy (Garnavich et al., 1998; Riess et al., 1998; Perlmutter et al., 1999; Tonry et al., 2003; Knop et al., 2003). The evidence for dark energy is supported by cross-cutting cosmological results, such as the measurement of the cosmic microwave background anisotropy, which indicates a flat universe (De Bernardis et al., 2000; Jaffe et al., 2001; Sievers et al., 2003; Spergel et al., 2003); the evolution in the number density of X-ray emitting galaxy clusters (Borgani et al., 2001; Henry , 2001; Schuecker et al., 2003) and galaxy redshift surveys (Efstathiou et al., 2002), indicate that $\Omega_M \approx 0.3$. Taken together, these independent measurements suggest a concordance universe $(\Omega_M,\Omega_\Lambda)=(0.3,0.7)$. However, the SN Hubble diagram remains the most direct approach currently in use for studying cosmic acceleration and, thus, systematic effects affecting the observed brightness, of type Ia supernovae should be carefully considered. These include: uncorrected host galaxy extinction (see e.g. Rowan-Robinson (2002)), dimming by photon-axion mixing over cosmological distances (Csaki et al., 2001; Deffayet et al., 2001; Mörtsell et al., 2002), dimming by intergalactic gray dust (Aguirre, 1999a,b; Mörtsell & Goobar, 2003) and intrinsic luminosity evolution (Drell et al., 2000).

Send offprint requests to: S. Nobili , serena@physto.se

This sentence should be re-written to make clear that we have already addressed the concerns of Rowan-Robinson with two papers (both Sullivan et al and Knop et al), which should both be cited here. And we do not want to cite Drell et al here, since they had simply made mistakes in their paper, which we have pointed out. Almost all of these issues were first raised and preliminarily addressed in P97 and P98, so we should cite them as well, and the go on to explain that we are now going to the next level of detailed study of these effects.

Add as the first reference here:
Perlmutter 1998 (Nature)
and replace this Garnavich 1998 paper with Garnavich, ApJLett, 493, L53 (1998).
[These were the first two papers that showed evidence for lambda in a flat universe.]

Determining cosmological distances through type Ia supernova fluxes at longer restframe wavelengths offers potential advantages, e.g. less sensitivity to dust along the line of sight, either in the host galaxy or in the intergalactic medium. On the other hand, the "standard candle" properties at these wavelengths and the possibility of additional systematic effects need to be investigated.

Using restframe *I*-band, the uncertainty due to extinction by dust is greatly reduced as compared with restframe *B*-band measurements. For example for Milky-Way type dust ($R_V = 3.1$) the ratio of extinction for the two bands is sizable, $A_B/A_I \sim 2-3$. In general, the extinction corrections become less sensitive to our knowledge of the intrinsic supernova colors and dust properties.

I-band lightcurves typically show a second peak 15-30 days after the first maximum. It has been suggested that the intensity and time-difference between the first and second *I*-band peak are related to the intrinsic luminosity of the type Ia SNe, appearing later and more evident for normal type Ia and earlier and fainter for subluminous ones (Hamuy et al., 1996a; Wang, 2003). Thus, building *I*-band lightcurves for type Ia supernovae offers the possibility of finding means for probing brightness evolution.

The scope of this work is to test the feasibility of using restframe *I*-band for cosmological distance measurements, using data available to date, and assess the importance of observing in this wavelength range for the future samples of SNe. For that purpose, we develop a template fitting technique to estimate the first ($I_{\rm max}$) and second ($I_{\rm sec}$) *I*-lightcurve peaks, which we apply to 42 nearby SNe Ia. $I_{\rm max}$ is used to build a SN Ia Hubble diagram reaching out to $z \sim 0.5$. Infrared data of a supernova at redshift $z = 0.543$, SN 2000fr, is presented and used in the Hubble diagram, together with other two SNe in the same reshift range, available in literature, SN 1999Q (Riess et al., 2000) and SN 1999ff (Tonry et al., 2003). The properties of the second peak in the restframe *I*-band lightcurves are investigated. Furthermore, additional color information is used to test for extinction by non-conventional dust for three $z \sim 0.5$ supernovae.

This subscript "sec" really looks like its the unit of time, "seconds." How about if we change it to "max2" -- short for "maximum #2"?

"two other"

the

2. I-band lightcurve fit

The second lightcurve peak seen in nearby type Ia SNe, varies in strength and position with respect to the primary maximum, and complicates the use of a single parametrized template for lightcurve fitting, which is currently often applied for *B* and *V*-band, (see e.g. Perlmutter et al. (1997); Goldhaber et al. (2001) for example of the timescale stretch factor approach).

We have developed a method for fitting *I*-band lightcurves using five free parameters. The underlying function is a combination of two standard *B*-band templates of type Ia supernovae[1]. Our fitting procedure can be summarized as follows: one *B*-band template is used to fit the time (t_1) and the first peak magnitude (I_1), together with a stretch factor (s_I), which is also applied to the second *B*-band template shifted in time to fit the time (t_2) and magnitude of the second peak (I_2). In general, $I = I_1\mathcal{B}(s_I(t-t_1)) + I_2\mathcal{B}(s_I(t-t_2))$, where $\mathcal{B}$ is the *B*-band lightcurve template. The five parameters fitted are thus: $\{t_1, t_2, I_1, I_2, s_I\}$, (see Table 1). A similar approach has also been proposed by Wang (2003) who calls it "super-stretch" to emphasize its extension of the stretch approach.

Contardo et al. (2000) proposed a model composed of as many as 4 functions for a total of 10 parameters in order to fit all *UBVRI*-bands. Their method used two Gaussian functions to fit the two peaks together with a straight line to fit the late time decline and an exponential factor for the pre-max rising part of the lightcurve. This method describes type Ia SNe lightcurve in all optical bands, though, as the authors recognize, does not represent accurately the second peak in the *I*-band due to the influence of the linear decline. However, the main disadvantage of their method is the large number of free parameters, thus the need for the object to be extremely well sampled.

The use of the standard *B*-band template of type Ia supernovae in place of the Gaussian function, reduces the number of free parameters by a factor of two. Moreover, with this choice, no additional functions are needed to fit the pre-max rising part of the lightcurve nor the late time decline. Implicitly, we have thus assumed that the rising part of the lightcurve in *I*-band is the same as in *B*-band. As our goal is only to measure the position and amplitude of the first two peaks, we limit the fit to 40 days after maximum, neglecting the late time decline. Note that, unless otherwise specified, the supernova phase always refers to the time relative to restframe *B*-band lightcurve maximum.

t_1	time of the peak of the first $\mathcal{B}$ template
I_1	peak magnitude of the first $\mathcal{B}$ template
t_2	time of the peak of the second $\mathcal{B}$ template
I_2	peak magnitude of the second $\mathcal{B}$ template
s_I	stretch factor of the time axis
$t_{\rm max}$	time of the first *I*-lightcurve peak
$I_{\rm max}$	first *I*-lightcurve peak magnitude
$t_{\rm sec}$	time of the second *I*-lightcurve peak
$I_{\rm sec}$	second *I*-lightcurve peak magnitude

Table 1 Summary of the parameters used in this work to describe the *I*-band lightcurve. The first five parameters are determined by fitting the data (see text for details). The next four parameters are the actual time and peak values of the lightcurve.

2.1. The data set

We applied this method to fit a sample of local SNe for which both *B* and *I*-band data are available in the litterature from the Calan/Tololo (Hamuy et al., 1996a), CfA (Riess et al., 1999) and CfA2 (Jha , 2002) data sets. Data from three other well studied individual supernovae were also included: SN 1989B (Wells et al., 1994), SN 1994D (Richmond et al., 1995) and one subluminous supernova: SN 1991bg. There are at least two available data sets in restframe *I*-band for SN 1991bg, one published by Filippenko et al. (1992) with quite good coverage from about 3 days after *B*-band maximum light to +60 days,

[1] The *B*-band template in Nugent et al. (2003) has been used.

another one published by Leibundgut et al. (1993) with four data points, the first of which is at the time of *B*-band maximum. The agreement between the two data sets was assessed by comparing the measurements taken at the same date, i.e. JD=2448607, where we found a difference of 0.06 mag. We take this as an estimate of the measurement uncertainty in data of Leibundgut et al. (1993) as no errors are reported in that work.

2.2. Fitting method and results

Only supernovae with at least 6 data points and a coverage in time constraining both peaks, were selected for lightcurve fitting. This resulted in a total of 42 SNe. Table 2 lists the parameters resulting from the fitting procedure. Note that the fit was performed in units of flux, while the parameters given in the table are transformed to magnitudes. Prior to fitting, all data points were K-corrected to restframe *I*-band as in (Kim et al., 1996; Nugent et al., 2003), assuming standard Bessel *I*-band and time information from the available *B*-band data. A new spectroscopic template was built for computing the *K*-corrections, that is a slightly modified version of the template found in Nugent et al. (2003). We have preserved the SED from the UV through the Si II 6150Å feature, following (Nobili et al., 2003), but redward of that we have incorporated additional spectra from the SCP Spring 1999 search (Aldering, 2000; Nugent & Aldering, 2000) to improve this region as the orginal template was sparse and required a lot of interpolation. A potential source of systematic uncertainties is in the *K*-corrections due to the wide Ca IR triplet absorption feature, found to vary considerably among Type Ia supernovae (Nugent et al., 2003). However, up to $z \sim 0.1$ the contribution of this feature is in general not critical to the precision of the *K*-corrections. For more distant SNe this could be a source of systematic uncertainty that has to be taken into account.

Note that the values of I_2 reported in Table 2 are not the actual magnitudes of the secondary peak , $I_{\rm sec}$, but a parameter indicating the size of the contribution of the secondary B-band template to the overall I-band template.

In Figure 1 all the fitted lightcurves are shown. They are sorted in chronological order, except for the two very subluminous supernovae: SN 1991bg and one of the supernovae in the CfA2 data-set, SN 1997cn, displayed at the bottom of the figure. As no date of *B*-band maximum light is known from the literature for SN 1997cn, the origin of the time axis was put to the epoch ($JD = 2450597.75$) when this supernova was first observed. Note that the second peak for the sub-luminous supernovae is almost completely absent, resulting in a value of $I_2 \sim 2.5$ to 3 magnitudes fainter than I_1.

Our sample also includes SNe that are classified as spectroscopic peculiar, showing similarities with the over-luminous SN 1991T (Li et al., 2001; Howell , 2001). These are SN 1995bd, SN 1997br, SN 1998ab, SN 1998es, SN 1999aa, SN 1999ac, SN 1999dq and SN 1999gp. One supernova, SN 1993H, was reported to show similarities with the spectrum of the peculiar under-luminous 1986G (Hamuy et al., 1993). However, not all of these show peculiarities in their *I*-band lightcurve shape when compared to spectroscopic normal SNe Ia. Recently, Krisciunas et al (2003), built the Hubble diagram for SNe Ia in infrared *J*, *H* and *K*-bands out to $z = 0.04$, and reported that three spectroscopic peculiar SNe, SN 1999aa, SN 1999ac and SN 1999aw, do not show a behavior different than that of normal SNe. In the attempt to assess the homogeneity of SNe as standard candles in the *I*-band, we choose not to exclude the peculiar SNe from our sample, and monitor possible deviant behavior of these objects.

Analyzing the results of our fits, we found that type Ia SNe show a variety of properties for the *I*-band lightcurve shape. In particular we noticed that the lightcurve could peak between -3 days and +3 days w.r.t. $B_{\rm max}$, as shown in Figure 2 (left panel). The time of the second peak, $t_{\rm sec}$ (relative to $B_{\rm max}$), is shown in the right panel. The distribution of $t_{\rm max}$ is centered at day -0.3 and has a dispersion of $\sigma = 1.3$ days. $t_{\rm sec}$ is centered at 23.6 with a dispersion of $\sigma = 4.4$ days.

The reduced χ^2 for the fits given in Table 2 are generally around unity, except for a few cases. In particular we note that SN 1994D has a $\chi^2/dof \sim 26$. The uncertainties for this supernova may be underestimated. But, even assuming them to be of the order of a few percent (see Knop et al. (2003)), the reduced χ^2 remained large, possibly indicating the limitations of the fitting template. As in other cases we find a systematic trend in the residuals, especially in the rising part of the lightcurves, that suggest this fitting model could be improved. It should be noted however, that this is not affecting the results reported in this work, as only a handful of SNe in our sample have data on the lightcurve rise.

While the χ^2 gives a measurement of the goodness of the fit, in the next section we test the robustness and accuracy of the parameter estimation in our fitting method, reported in Table 2.

2.3. Monte-Carlo tests of the fitting method

Given the heterogeneous origin of the data sample, the quality and the sampling of the individual SN lightcurves vary considerably. Only a few supernovae have excellent time coverage in the *I*-band, resulting in a wide range of accuracy in the fitted parameters. The robustness of the fitting procedure was tested for all circumstances of data quality and time sampling in our sample by means of Monte Carlo simulations. We generated 1000 sets of simulated lightcurves for each supernova. The synthetic data points had the same time sampling as the real lightcurves and with deviations from the best fit template by randomization according to the measurement errors (assumed Gaussian). The simulated lightcurves were fitted using the same method as for the experimental data sets. The distribution of the fitted parameters on the simulated data was used to compare with the input data from the fits of the experimental data. The mean value in the distribution of each parameter coincide generally with those expected within one standard deviation, not giving evidence for biases. This lends confidence that the fitting procedure is robust, and given the model of the lightcurve template will not yield biased estimations of the parameters. However, of 42 supernovae, 2 cases showed significant deviations, both identified as spectroscopic peculiar SNe,

SN	z	s_I	t_1	I_1	t_2	I_2	χ^2/dof
1989B[1]	0.002	1.100 ± 0.126	-0.590 ± 1.549	11.752 ± 0.059	23.123 ± 2.079	12.513 ± 0.175	0.51
1991bg[4]	0.005	1.104 ± 0.034	3.274 ± 0.380	13.521 ± 0.006	28.800 ± 1.123	16.506 ± 0.122	1.45
1992al[4]	0.015	0.952 ± 0.054	1.176 ± 1.016	15.039 ± 0.043	27.887 ± 1.078	15.527 ± 0.069	0.12
1992bc[4]	0.020	1.121 ± 0.030	-1.579 ± 0.146	15.639 ± 0.014	27.677 ± 0.492	16.510 ± 0.026	1.25
1992bg[4]	0.035	0.963 ± 0.065	0.257 ± 1.929	17.543 ± 0.086	26.392 ± 2.543	17.963 ± 0.060	1.59
1992bh[4]	0.045	1.086 ± 0.145	-0.008 ± 1.029	17.899 ± 0.028	26.766 ± 2.494	18.543 ± 0.116	0.83
1992bo[4]	0.019	0.952 ± 0.019	-0.609 ± 0.162	16.064 ± 0.016	23.403 ± 0.374	16.944 ± 0.042	3.38
1992bp[4]	0.079	0.891 ± 0.053	-0.292 ± 0.710	18.962 ± 0.029	27.750 ± 1.287	19.346 ± 0.084	1.13
1993ag[4]	0.049	0.924 ± 0.058	1.092 ± 0.863	18.384 ± 0.039	26.904 ± 2.010	18.759 ± 0.060	0.37
1993H[4]	0.024	0.953 ± 0.033	-2.072 ± 0.960	16.664 ± 0.040	20.556 ± 0.943	17.532 ± 0.048	2.95
1993O[4]	0.051	1.089 ± 0.080	0.462 ± 0.917	18.197 ± 0.023	26.248 ± 1.108	18.858 ± 0.034	1.45
1994ae[3]	0.004	1.051 ± 0.017	-1.110 ± 0.142	13.383 ± 0.018	26.664 ± 0.312	14.032 ± 0.042	1.51
1994D[2]	0.002	0.891 ± 0.004	-1.007 ± 0.043	12.177 ± 0.004	25.219 ± 0.091	12.836 ± 0.008	26.01
1994M[3]	0.023	0.945 ± 0.041	0.035 ± 1.262	16.513 ± 0.050	24.824 ± 1.027	17.139 ± 0.063	3.34
1994T[3]	0.035	0.740 ± 0.026	2.371 ± 1.319	17.458 ± 0.049	30.187 ± 0.988	17.840 ± 0.053	3.07
1995al[3]	0.005	1.158 ± 0.046	-1.002 ± 0.472	13.526 ± 0.022	24.696 ± 0.751	14.149 ± 0.057	0.79
1995bd[3]	0.016	1.166 ± 0.025	-0.095 ± 0.112	16.082 ± 0.012	26.516 ± 0.367	16.632 ± 0.060	1.88
1995D[3]	0.007	1.267 ± 0.054	-1.408 ± 0.682	13.708 ± 0.026	24.763 ± 0.744	14.454 ± 0.037	0.52
1995E[3]	0.012	1.026 ± 0.040	0.067 ± 0.635	15.393 ± 0.024	26.340 ± 0.950	16.093 ± 0.050	0.75
1996ai[3]	0.003	1.115 ± 0.024	-2.042 ± 0.495	13.986 ± 0.022	24.947 ± 0.504	14.675 ± 0.023	9.68
1996bl[3]	0.036	0.942 ± 0.026	1.932 ± 0.365	17.079 ± 0.022	29.619 ± 0.684	17.702 ± 0.033	2.36
1996bo[3]	0.017	1.072 ± 0.010	-0.325 ± 0.113	15.701 ± 0.005	24.675 ± 0.186	16.253 ± 0.013	12.25
1996C[3]	0.030	1.059 ± 0.038	0.278 ± 1.085	16.829 ± 0.052	27.206 ± 0.928	17.521 ± 0.030	3.84
1996X[3]	0.007	1.079 ± 0.041	-1.944 ± 0.371	13.399 ± 0.012	24.524 ± 0.774	14.170 ± 0.033	0.79
1997bp[5]	0.008	1.235 ± 0.049	1.092 ± 0.277	14.134 ± 0.006	25.847 ± 0.484	14.637 ± 0.018	1.36
1997bq[5]	0.009	1.014 ± 0.014	0.479 ± 0.099	14.580 ± 0.017	25.130 ± 0.230	15.139 ± 0.017	2.71
1997br[5]	0.007	1.349 ± 0.035	0.769 ± 0.110	13.683 ± 0.020	20.672 ± 0.451	14.295 ± 0.037	2.75
1997cn[5]	0.017	0.840 ± 0.049	-1.711 ± 0.776	16.426 ± 0.027	24.070 ± 1.067	18.255 ± 0.156	1.68
1997dg[5]	0.031	0.965 ± 0.060	-1.324 ± 1.082	17.240 ± 0.035	26.675 ± 2.351	17.744 ± 0.051	1.18
1997e[5]	0.013	0.931 ± 0.031	-1.375 ± 0.315	15.477 ± 0.007	23.879 ± 0.386	16.064 ± 0.022	2.87
1998ab[5]	0.027	1.413 ± 0.046	0.279 ± 0.179	16.485 ± 0.021	19.787 ± 0.556	17.049 ± 0.042	1.68
1998dh[5]	0.009	0.997 ± 0.011	-0.337 ± 0.169	14.099 ± 0.015	26.025 ± 0.275	14.682 ± 0.024	0.77
1998es[5]	0.011	0.980 ± 0.140	-2.309 ± 0.511	14.083 ± 0.016	24.278 ± 1.062	14.928 ± 0.085	1.15
1998v[5]	0.018	0.940 ± 0.036	0.545 ± 0.611	15.790 ± 0.017	25.688 ± 0.698	16.100 ± 0.056	4.82
1999aa[5]	0.014	1.288 ± 0.014	0.301 ± 0.072	15.242 ± 0.007	25.585 ± 0.180	15.871 ± 0.027	8.16
1999ac[5]	0.009	1.210 ± 0.027	1.328 ± 0.283	14.321 ± 0.006	23.045 ± 0.519	15.057 ± 0.032	1.61
1999cl[5]	0.008	0.970 ± 0.118	-0.107 ± 0.571	13.139 ± 0.022	22.206 ± 1.647	13.688 ± 0.101	0.21
1999dq[5]	0.014	1.179 ± 0.024	-0.324 ± 0.126	14.785 ± 0.006	25.492 ± 0.198	15.312 ± 0.013	2.28
1999gp[5]	0.027	1.261 ± 0.044	-1.600 ± 0.263	16.405 ± 0.008	26.011 ± 0.526	17.045 ± 0.024	1.25
2000cn[5]	0.023	0.799 ± 0.026	-0.362 ± 0.206	16.679 ± 0.015	23.965 ± 0.441	17.256 ± 0.062	2.20
2000dk[5]	0.017	0.809 ± 0.016	-1.342 ± 0.177	15.767 ± 0.007	24.297 ± 0.429	16.222 ± 0.048	5.08
2000fa[5]	0.021	1.119 ± 0.050	-0.235 ± 0.278	16.289 ± 0.037	24.911 ± 0.423	16.888 ± 0.111	0.10

Table 2 Results of the *I*-band lightcurve fit of 42 nearby supernovae: t_1 and I_1 are the parameters for the time and amplitude fitted on the first *B*-band template, t_2 and I_2 are the parameters for the time and amplitude fitted on the second *B*-band template, and s_I is the stretch factor. The data were taken from: [1] Wells et al. (1994); [2] Richmond et al. (1995); [3] Riess et al. (1999); [4] Hamuy et al. (1996a); [5] Jha (2002); [6] Filippenko et al. (1992); Leibundgut et al. (1993).

– SN 1997br: in about 3% of the cases we found $\chi^2/dof \geq 7$. These cause the distributions to have different standard deviation than what is computed as uncertainty by the fitting procedure. Excluding them results in the expected distributions.
– SN 1998ab: the simulated data sets result in two populations of parameters, which reduces to one when imposing a cut on $\chi^2/dof \leq 6$. Note that about 78% of the simulations satisfy this condition.

In both cases a cut of the tail of the χ^2 distribution was enough to discriminate between the results, thus these supernovae were kept in the remaining analysis since the χ^2/dof of the fits to the real data fulfilled these criteria.

For the rest of the supernovae, the simulations confirmed the expected parameters, giving general confidence in the robustness of the procedure and the accuracy of the uncertainties on the parameters given in Table 2.

2.4. Intrinsic variations

We investigated possible relations between *I*-band and *B*-band parameters. Published *B*-band data, when avalaible, was fitted

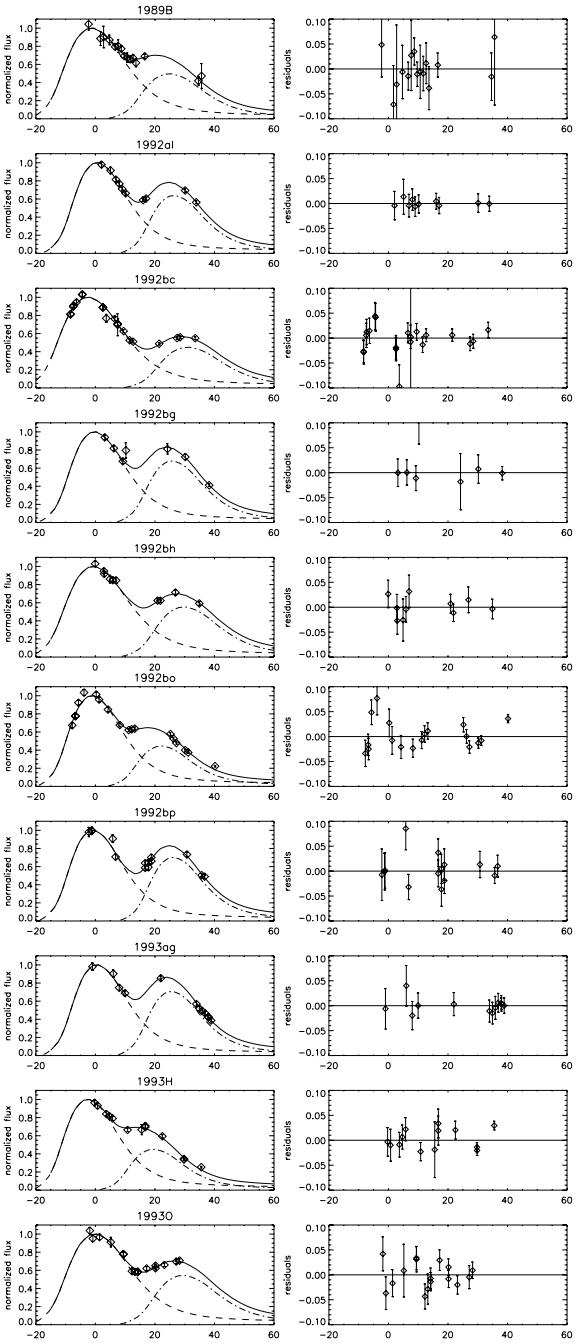

Fig. 1 *I*-band lightcurve fits. On the ordinate is the flux normalized to the first peak, on the abscissa the restframe time since *B*-band maximum. The dashed line and the dash-dotted line represent the two *B*-band templates used to fit the first and second peak respectively.

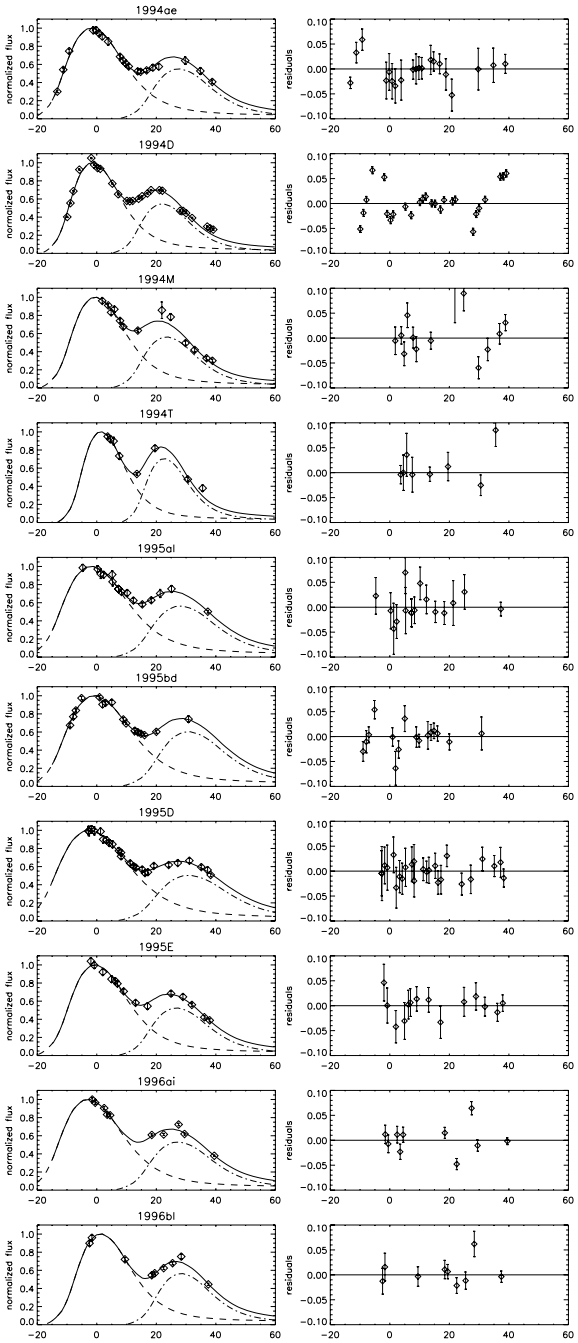

Fig. 1 continued. *I*-band lightcurve fits. On the ordinate is the the flux normalized to the first peak, on the abscissa the restframe time since *B*-band maximum. The dashed line and the dash-dotted line represent the two *B*-band templates used to fit the first and second peak respectively.

using a template in order to determine the time of maximum luminosity, the stretch factor, s_B, and the amplitude of maximum, m_B, following Goldhaber et al. (2001). A width-luminosity relation was found for the first *I*-band lightcurve peak. Figure 3 shows the *I*-band absolute magnitude versus the stretch factor in *B*-band for SNe with $z_{CMB} \geq 0.01$, where the distance (in Mpc) to each SN was calculated from its redshift, assuming a value for the Hubble constant, $H_0 = 72$ km s^{-1} Mpc^{-1}. The error bars in Figure 3 include an uncertainty of 300 km/s on the redshifts from the possible peculiar velocities of the host galaxies. Corrections for Milky Way and host galaxy extinction were also applied, i.e.

$$M^I_{\max} - 5\log(H_0/72) = I_{\max} - A^{MW}_I - A^{host}_I - 25 - 5\log(d_L)$$

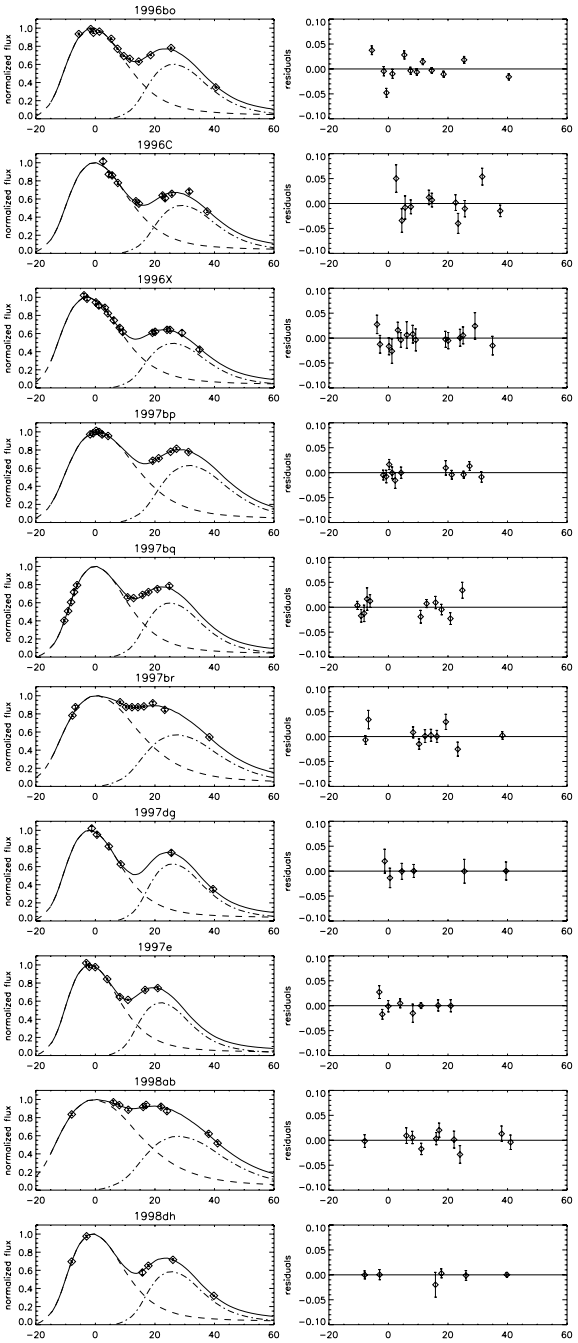

Fig. 1 continued. *I*-band lightcurve fits. On the ordinate is the flux normalized to the first peak, on the abscissa the restframe time since *B*-band maximum. The dashed line and the dash-dotted line represent the two *B*-band templates used to fit the first and second peak respectively.

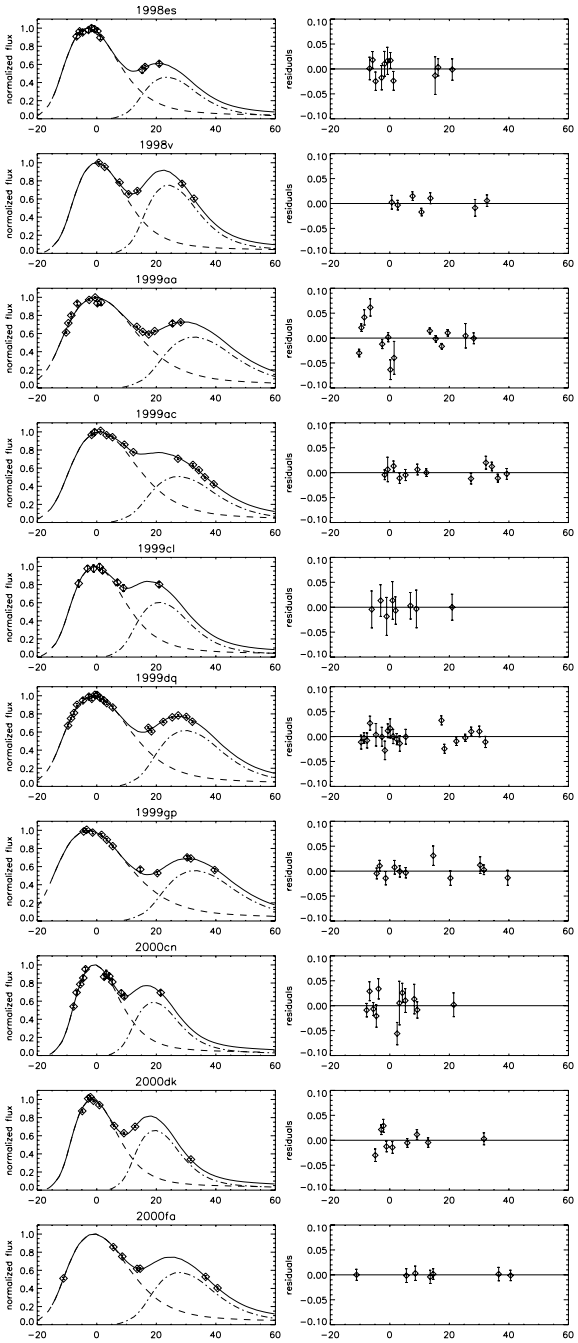

Fig. 1 continued. *I*-band lightcurve fits. On the ordinate is the flux normalized to the first peak, on the abscissa the restframe time since *B*-band maximum. The dashed line and the dash-dotted line represent the two *B*-band templates used to fit the first and second peak respectively.

The host galaxy extinction corrections applied to most of the supernovae are determined as weighted average of the three estimates given in Table 2 of Phillips et al. (1999), and assuming $R_I = 1.82$. The extinction for the supernovae in the CfA2 data set was calculated following the same procedure, using *B* and *V*-band photometry. SN 1995E has been excluded from the sample as it is highly extincted (see also discussion in Nobili et al. (2003)). Two supernovae in the sample, the spectroscopic peculiar SN 1998es and SN 1999dq, plotted with filled symbols in Figure 3, appear intrinsically redder than average, and become $\sim 2-3\sigma$ deviant from average after correction for host galaxy extinction. Before introducing lightcurve shape corrections, the spread measured in the $M^I_{\rm max}$ excluding these two SNe, is about 0.24 mag (0.28 mag if they are included). The

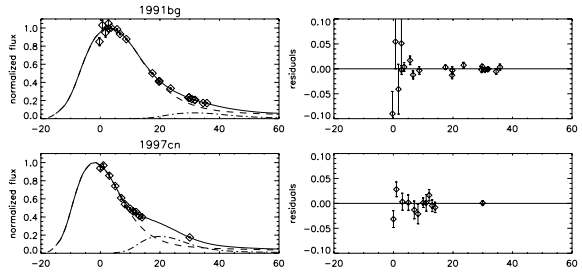

Fig. 1 continued. *I*-band lightcurve fits of the under-luminous supernovae SN 1991bg and SN 1997cn. The dashed line and the dash-dotted line represent the two *B*-band templates used to fit the first and second peak respectively. Note that the second peak is fitted as ∼ 3 mag fainter than the first peak.

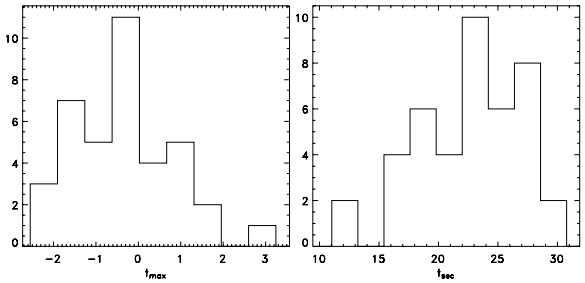

Fig. 2 Distribution of the time of *I*-band maximum referred to the time of *B*-band maximum (left panel) and the distribution of the time of second maximum referred to the time of *B*-band maximum (right panel).

solid line shows the best fit to the data, obtained for a slope $\alpha_I = 1.18 \pm 0.19$ and an absolute magnitude for a stretch $s_B = 1$ supernova equal to $M^I_{\rm max}(s_B = 1) = -18.84 \pm 0.03$ mag [2]. The dispersion measured as r.m.s. on the data along the fitted line is 0.17 ± 0.03 mag. A similar correlation was found between the peak magnitude and the stretch in *I*-band, s_I, with an r.m.s. of ∼ 0.19 mag, about the best fit line, obtained excluding SN 1998es and SN 1999dq.

A correlation was found between $t_{\rm sec}$ and the stretch factor in *B*-band, as shown in Figure 4. There are three outliers labeled in the figure, SN 1993H , SN 1998es and SN 1999ac, which are identified as spectroscopically peculiar supernovae. However, other supernovae in our sample also classified as spectroscopically peculiar, behave as "normal" type Ia SNe. A linear fit to the data was done, excluding the outlier SNe.

Figure 5 shows a possible correlation found between $I_{\rm sec}$, ~~corrected~~ for the luminosity distance and both Galaxy and host galaxy extinction, and the stretch s_B, at least for $s_B < 0.9$. This correlation, however, disappears for larger values of s_B.

All of these correlations, shown in Figure 3 - 5, were expected since it has been suggested that the location and the intensity of the secondary peak depends on the *B*-band intrinsic luminosity of the supernova (Hamuy et al., 1996a).

Figure 6 shows the *I*-band stretch, s_I, plotted versus *B*-band stretch, s_B, where some of the supernovae, which are spectroscopically peculiars, are somewhat deviant from the correlation found.

We have investigated the possible existence of further relations between the fitted parameters, but found no statistically significant correlations.

[2] The value fitted for $M^I_{\rm max}$ depends on the value assumed for the Hubble parameter, $H_0 = 72$ km s^{-1} Mpc^{-1}. However, its value is not used in any of the further analysis presented in this paper.

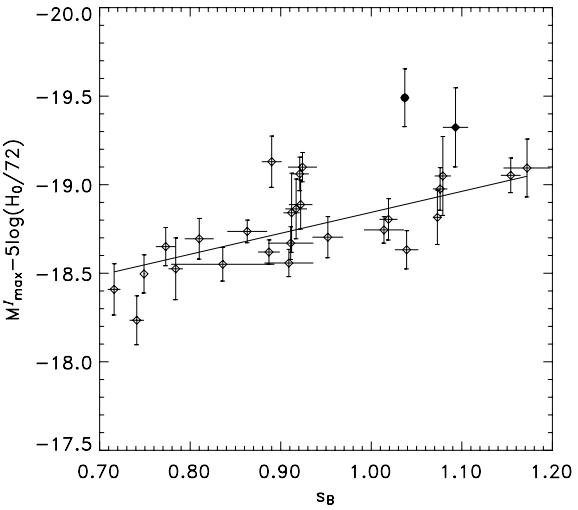

Fig. 3 *I*-band absolute magnitude versus stretch in B-band. The best fit gives $\alpha_I = 1.18 \pm 0.19$ and $M^I_{\rm max}(s_B = 1) = -18.84 \pm 0.03$ mag. The two deviating supernovae, SN 1998es (filled diamond) and SN 1999dq (filled circle), were excluded from the fit.

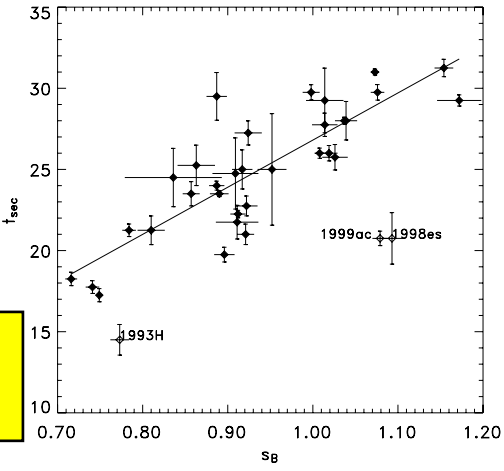

Fig. 4 Time of the second peak since $B_{\rm max}$ vs the stretch in *B*-band. The supernovae labelled are all classified as spectroscopically peculiar.

3. The *I*-band Hubble Diagram

The fitted values of $I_{\rm max}$ were used to build a Hubble diagram in *I*-band. A total of 28 supernovae of the sample considered

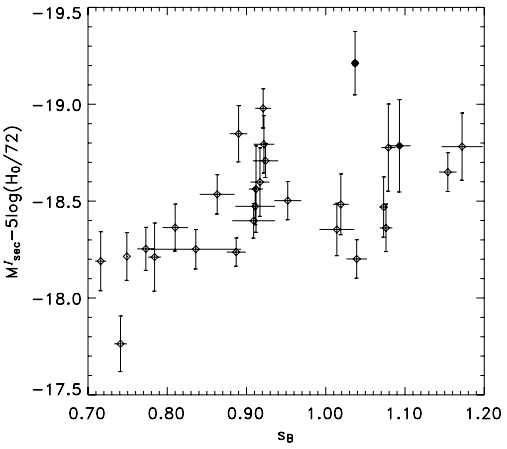

Fig. 5 Absolute magnitude of the secondary peak versus the stretch in *B*-band. The two deviating supernovae in Figure 3 are SN 1998es (filled diamond) and SN 1999dq (filled circle).

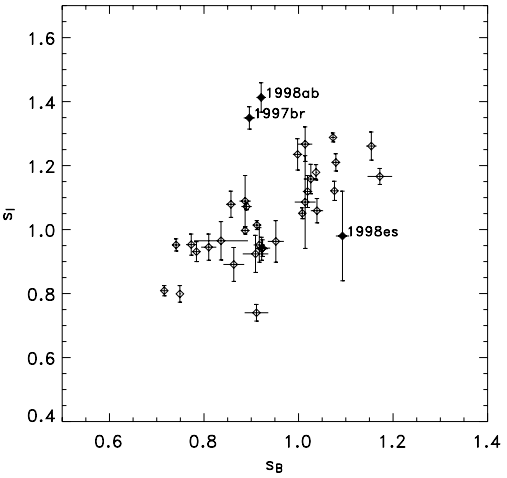

Fig. 6 *I*-band lightcurve stretch, s_I, versus *B*-band stretch, s_B. The labeled supernovae are somewhat deviant from the correlation shown by the ensamble. SN 1998ab, SN 1997br and SN 1998es are classified as peculiar.

here are in the Hubble flow having a redshift $z_{CMB} \geq 0.01$[3]. The maximum redshift in this sample is 0.1.

The width-luminosity relation found between the fitted absolute *I*-band magnitude and the *B*-band stretch factor was used to correct the peak magnitude, with a $\alpha_I = 1.18 \pm 0.19$ as measured in the previous section, similarly to what is usually done in *B*-band (Perlmutter et al., 1999). The peak magnitude was also corrected for Milky Way and for host galaxy extinction:

$$m_I^{\rm eff} = m_I + \alpha_I(s_B - 1) - A_I^{host} - A_I^{MW} \quad (1)$$

[3] The lower limit chosen in previous works by the SCP is slightly higher. However, we include these lower redshift SNe in the sample in order to increase the statistical significance. Cutting the Hubble diagram above $z = 0.015$ would in fact, decrease the sample by about a 30 %. Note however, that this choice does not affect significantly any of the results.

SN	s_B	z_{CMB}	$m_I^{\rm eff}$
1992al	0.917 ± 0.012	0.014	14.868 ± 0.162
1992bc	1.076 ± 0.008	0.020	15.718 ± 0.111
1992bg	0.952 ± 0.017	0.036	17.120 ± 0.107
1992bh	1.014 ± 0.022	0.045	17.637 ± 0.062
1992bo	0.741 ± 0.008	0.017	15.710 ± 0.138
1992bp	0.863 ± 0.022	0.079	18.689 ± 0.055
1993H	0.773 ± 0.011	0.025	16.169 ± 0.106
1993O	0.887 ± 0.012	0.053	17.967 ± 0.054
1993ag	0.909 ± 0.027	0.050	17.928 ± 0.069
1994M	0.810 ± 0.016	0.024	16.080 ± 0.111
1994T	0.911 ± 0.025	0.036	17.105 ± 0.085
1995bd	1.172 ± 0.026	0.014	14.939 ± 0.162
1996C	1.039 ± 0.013	0.027	16.669 ± 0.097
1996bl	0.924 ± 0.016	0.035	16.630 ± 0.070
1996bo	0.890 ± 0.011	0.016	14.860 ± 0.138
1997bq	0.912 ± 0.009	0.010	14.154 ± 0.219
1997dg	0.836 ± 0.057	0.030	16.740 ± 0.110
1997E	0.784 ± 0.008	0.013	14.888 ± 0.173
1998ab	0.921 ± 0.010	0.028	16.180 ± 0.083
1998es	1.093 ± 0.014	0.010	13.885 ± 0.219
1998V	0.922 ± 0.013	0.017	15.272 ± 0.131
1999aa	1.073 ± 0.005	0.015	15.250 ± 0.146
1999ac	1.079 ± 0.009	0.010	14.144 ± 0.218
1999dq	1.037 ± 0.000	0.014	14.382 ± 0.155
1999gp	1.154 ± 0.011	0.026	16.303 ± 0.090
2000cn	0.749 ± 0.000	0.023	16.114 ± 0.107
2000dk	0.716 ± 0.007	0.016	15.375 ± 0.147
2000fa	1.019 ± 0.010	0.022	16.029 ± 0.106

Table 3 List of SNe used in the Hubble diagram. $m_I^{\rm eff}$ is the peak magnitude corrected for the dust extinction and for the width-luminosity relation, following Eq. 1. The quoted uncertainties do not include the redshift contribution due to peculiar velocities in the host galaxies, assumed equal to 300 km/s.

The effective magnitude, $m_I^{\rm eff}$ for the nearby supernovae, listed in Table 3, have been used for building the Hubble diagram in *I*-band, shown in Figure 7. The inner error bars include an uncertainty on the redshifts due to peculiar velocities in the host galaxies, assumed to be 300 km/s.

[missing space between "to" and "be"]

The solid line represents the best fit to the data for the concordance model $\Omega_M = 0.3$ and $\Omega_\Lambda = 0.7$. The fitted parameter, $\mathcal{M}_I$, is defined (as in Perlmutter et al. (1997)) to be

$$\mathcal{M}_I \equiv M_I - 5\log H_0 + 25 \quad (2)$$

where M_I is the *I*-band absolute magnitude for a *B*-band stretch $s_B = 1$ supernova. The two redder supernovae, SN 1998es and SN 1999dq, were excluded from the fit, and are plotted with different symbols in Figure 7. The value fitted is $\mathcal{M}_I = -3.19 \pm 0.03$. In order to disentangle the intrinsic dispersion from the statistical scatter due to the measurement uncertainties, we simulated data sets with a dispersion given by the measurement uncertainty only. Since the uncertainty due to peculiar motion in the host galaxy is dominant a very low redshift (~0.2 mag for z =0.01), we limited this calculation only to 15 SNe with z > 0.025, which correspond to an uncertainty of the same order as the measurement uncertainties in our sample. The average of the r.m.s. measured on each of the simulated data sets

"at"

is subtracted (geometrically) to the dispersion measured on the data, resulting in $\sigma = 0.13$ mag. We consider this an estimate of the intrinsic dispersion of the stretch corrected *I*-band lightcurve maximum, which agrees with the estimate given by Hamuy et al. (1996b) using 26 SNe of the Calan/Tololo sample. The estimated intrinsic uncertainty of 0.13 mag has been added in quadrature to the outer error bars of the plotted data. Note that if no correction $\alpha_I(s_B - 1)$ is applied the dispersion in the Hubble diagram becomes 0.24 ± 0.04 mag, somewhat smaller than the corresponding dispersion measured in the "uncorrected" *B*-band Hubble diagram. Moreover, we computed the dispersion in the Hubble diagram for the three data sets separately. Table 4 lists for each sample, the average redshift, the number of SNe, the weighted mean and standard deviation of the residuals in the Hubble diagram.uncertainty. The latter is dominated by the A similar weighted standard deviation was measured in the Calan/Tololo and CfA2 sample, while a larger value was found in the the CfA sample, though it is consistent within the uncertainties with the values for the other two samples (see Table 4). A small offset, -0.09 ± 0.12 mag, was measured in the CfA sample to the best fit model, however, this is compatible with statistical fluctuations. The weighted standard deviation would decrease slightly to 0.25 ± 0.06 if the Hubble diagram was built on this sample only.

The end of this sentence is missing.

4. High redshift supernovae

Next, we explore the possibility of extending the Hubble diagram to higher redshifts, where the effects of the energy density components of the universe are, in principle, measurable. The restframe *I*-band data available to date for this purpose is unfortunately very limited. It consists of only three supernovae at redshift $z \sim 0.5$ observed in the near infrared (NIR) J-band collected during three different campaigns conducted using different facilities and by two different teams. Keeping all of these sources of systematic errors in mind, we include the three supernovae in the Hubble diagram to show its potential and complementary with respect to the standard *B*-band Hubble diagram.

The following sections describe the three high redshift supernovae, SN 2000fr, SN 1999ff and SN 1999Q, and the lightcurve fitting procedure used.

4.1. SN 2000fr

SN 2000fr was discovered by the Supernova Cosmology Project (SCP) during a search for type Ia supernovae at redshift $z \sim 1$ conducted in *I*-band with the CFH-12k camera on the Canada-France-Hawaii Telescope (CFHT). The depth of the search allowed us to discover this supernova during its rise time about 11 rest-frame days before maximum B-band light.

insert: "z ~ 0.5"

The supernova type was confirmed with two spectra taken at the Keck II telescope and VLT, showing that it was a normal type Ia at $z = 0.543$, see Lidman et al. (2004); Garavini et al. (2004) for an extensive analysis of the spectrum. This supernova was followed-up in restframe *B*, *V* and *I* filters involving both ground and space based facilities. Approximately one year later, when SN 2000fr had faded sufficiently, infrared and optical images of the host galaxy without SN were obtained. The optical lightcurves, (Knop et al., 2003), have been fitted again, using the improved spectral templates, yielding a stretch parameter $s_B = 1.034 \pm 0.013$ and a time of $B_{\max} = 51685.6$. Restframe $B - V$ measurements at the time of $B_{\max}$ indicates that SN 2000fr did not suffer for reddening due to dust in the host galaxy, (see also Section 6 for a more extensive discussion). The Milky Way reddening is $E(B - V) = 0.030$ mag (Schlegel et al., 1998).

the

insert: ", tmax ="

The near-infrared data was collected with ISAAC at the VLT telescope. It consists of J_s-band observations during three epochs and a final image of the host galaxy without the SN (see Table 5). Each data point is made of a series of 20 to 60 images with random offsets between exposures. The observations were done in the J_s filter, which is narrower than other *J*-band filters. Figure 8 shows a comparison between J_s and *J* Persson filters, together with the atmospheric transmission, and the spectral template at maximum.

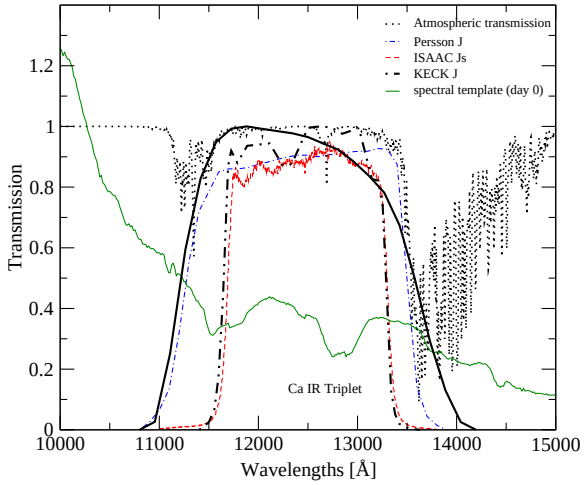

Fig. 8 Comparison between the standard *J* Persson filter, the J_s filter at ISAAC used for the observations of SN 2000fr and the *I*-band redshifted to z=0.543. The atmospheric transmission is also plotted. The spectral template at day 0 is on an arbitrary flux scale for readibility purpose.

Caption should refer to each of the curves, and say which is which (e.g., add the words "(heavy solid line)" after "I band redshifted to z=0.543" and "(dot-dashed line)" after Keck, etc.

The advantage in using a narrow *J* filter is that its transmission function cuts off entirely the region of strong atmospheric absorption between 13500 and 15000 Å. Consequently, the zero-point is significantly more stable than the one of standard *J*. This was very useful, because all of the ISAAC data was taken in queue mode, where typically only one or two standard stars are observed during a night, chosen from the list of Persson et al. (1998). All data, except the reference images, were taken during photometric nights and the difference in the zero-points from one night to the next were less than 0.01 magnitudes.

The data was reduced using both internally developed routines and the XDIMSUM package in IRAF[4]. The results were

[4] IRAF is distributed by the National Optical Astronomy Observatories, which are operated by the Association of Universities

	$\langle z \rangle$	n	$\overline{x}_w$ [a]	σ_w [b]
Calan/Tololo	0.038 (0.021)	9	0.04 ± 0.05	0.12 ± 0.06
CfA	0.025 (0.009)	6	-0.09 ± 0.12	0.26 ± 0.07
CfA2	0.018 (0.007)	11	-0.02 ± 0.05	0.15 ± 0.06

Table 4 Dispersion measured in the Hubble diagram for each of the sample, corrected for the width-luminosity relation; $\langle z \rangle$ is the average redshift of the sample, and its standard deviation given between brackets; n is the number of data points; $\overline{x}_w$ and σ_w are weighted mean and standard deviation of residuals in the Hubble diagram about the best fit model to the whole data sample.

[a] If R_i are residuals in the Hubble diagram and w_i are the weights, then
$\overline{x}_w = \sum w_i R_i / \sum w_i \pm m_{w2} / \sqrt{n_{eff}}$
$m_{w2} = \sum w_i R_i^2 / \sum w_i$
$n_{eff} = \sum {w_i}^2 / \sum w_i^2$

[b] $\sigma_w = m_{w2} \pm \sqrt{(m_{w4} - m_{w2}^2)/4 n_{eff} m_{w2}}$

MJD	Epoch	J_s(mag)	I(mag)
51685.06	-0.33	22.50 ± 0.09	23.52 ± 0.10
51709.02	15.20	23.57 ± 0.22	24.52 ± 0.23
51731.96	30.07	23.14 ± 0.15	23.99 ± 0.16

Table 5 Summary of J_s data for SN 2000fr. The quoted errors are due to statistical Poisson noise and the uncertainty on the ZP (contributing for 0.01 mag). Epochs are in restframe relative to B-band maximum. Restframe I-band is obtained through cross-filter K-correction from the observed J_s-band to Bessel I-band, and adding the offset found between optical and IR systems. The uncertainties also include the contribution from K-corrections, estimated to be 0.05 mag at all epochs considered.

found in agreement within the quoted uncertainties. The supernova images where aligned with the host galaxy images and flux scaled to the one with best seeing, using the field stars before performing PSF photometry. The results are given in Table 5. The stated uncertainties include the statistical Poisson noise and the uncertainty on the estimate of the zero point, added in quadrature.

The J_s-band magnitude takes into account a color term which arises from the difference between the J filter of the standard star system and the J_s filter used in ISAAC. This correction was small ~ 0.012 mag.

The cross-filter K-correction, K_{IJ_s}, to convert from J_s-band to rest-frame I-band, has been calculated following Kim et al. (1996) using the spectral templates improved for this work. However, an extra term has been added to the usual formula, in order to take into account the appropriate transformation between IR and optical photometric systems. The K-correction between filter x and y is given by $K'_{xy} = K_{xy} - (x - y)$, where $(x - y)$ is the color of Vega and K_{xy} is defined in Kim et al. (1996). Using the Vega magnitudes in I and J (Bessell et al., 1998; Cohen et al., 2003) and the 2MASS filter definition, we found the extra term to be $(I - J) = 0.03(\pm 0.02)$. This correction was applied when trasforming from the observed IR band to restframe I-band. We assumed 0.05 mag total uncertainty in the K-corrections.

for Research in Astronomy, Inc., under cooperative agreement with the National Science Foundation.

4.2. SN 1999ff

SN 1999ff was discovered by the High-Z Supernova Search Team (HZT) during a search conducted at CFHT using the CFH-12k camera in I-band (Tonry et al., 2003).[5] The supernova was confirmed spectroscopically as a type Ia at redshift $z = 0.455$. The Milky Way reddening is $E(B-V) = 0.025$ mag (Schlegel et al., 1998).

J-band observations, corresponding to restframe I-band, reported in the paper, were taken at Keck using NIRC in two epochs only. The J-band filter available at Keck is very similar to the ISAAC-J_s, shown in Figure 8. We have used the published observed photometry, and, for consistency with the treatment of both the low redshift supernovae and SN 2000fr, we computed the K-corrections using the improved spectral templates. We found differences with the results published in Tonry et al. (2003), due to the use of an incorrect filter in those calculations (Brian Schmidt, private communication). The I-band magnitudes were also corrected for the offset found between the optical and IR systems, as explained in the previous section. The restframe I-band magnitudes obtained this way are reported in Table 6. The published optical R-band data were used to fit restframe B-band lightcurve using the stretch method. The time of maximum was confirmed within 1 day with a best fit for the stretch $s_B = 0.80 \pm 0.05$.

MJD	Epoch	I(mag)
51501.29	5.01	23.57 ± 0.11
51526.31	22.21	24.06 ± 0.24

Table 6 Summary of IR data of SN 1999ff. Epochs are in restframe relative to B-band maximum ($MJD_{\max} = 51494.8$); restframe I-band magnitudes are computed applying K-corrections to the observed J-band data published in Tonry et al. (2003), and adding the offset found between optical and IR systems. The uncertainties also include the contribution from K-corrections, estimated to be 0.05 mag at all epochs considered.

[5] Another supernova, SN 1999fn, was followed in J-band by the HZT during the same search. However since it was found in a highly extincted Galactic field, E(B-V)=0.32 mag, and since it was strongly contaminated by the host galaxy, we did not include it in our analysis.

the

Has this wording been checked with Brian Schmidt yet? Very important to do before submitting.

This term is in Kim et al.'s definition of K_IJ already, since it already includes the zeropoint difference between the photometric systems used.

Is there any very short reason we can give for using 0.05 mag here?

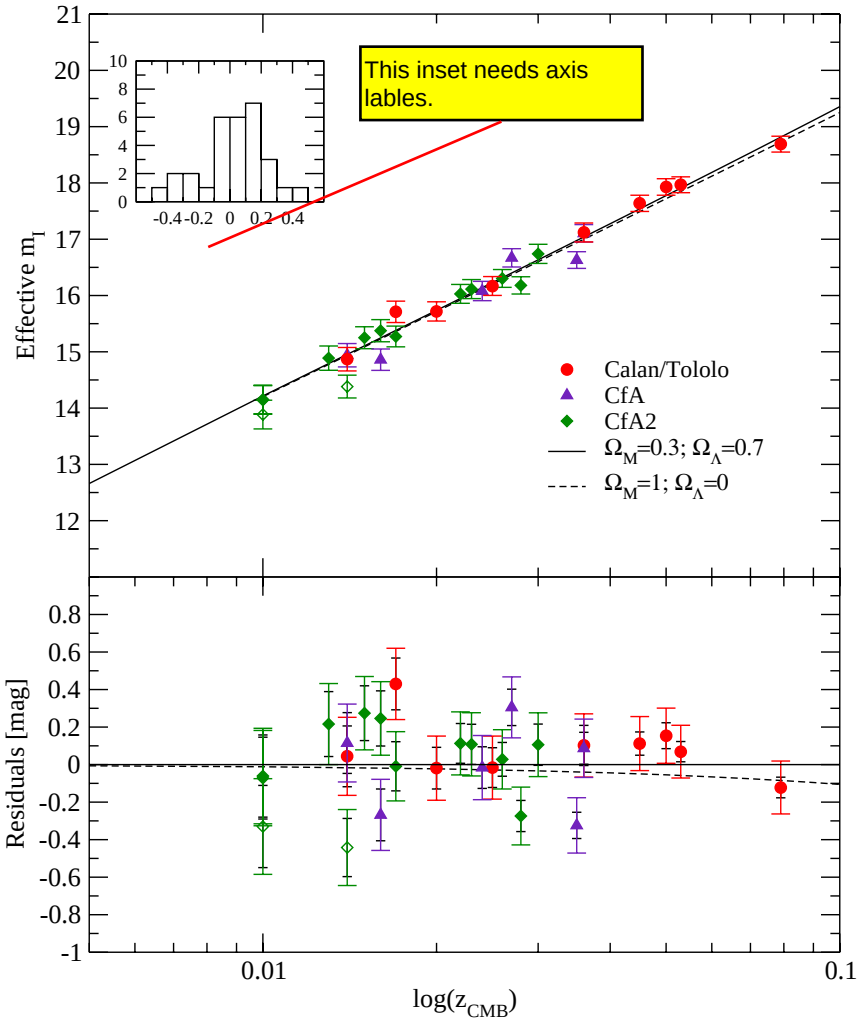

Caption should say what the inset plot shows.

Fig. 7 Effective *I*-band maximum vs redshift for the nearby supernovae of the Calan/Tololo, CfA and CfA2 sample. The data have been corrected for the stretch-luminosity relation and for Milky Way and host galaxy extinction. The r.m.s. along the concordance model line is $\sigma = 0.17 \pm 0.04$ mag. Subracting the contribution of the average uncertainty, results in 0.13 mag estimated intrinsic dispersion (see text for details). SN 1998es and SN 1999dq were excluded from the fit (see text) and are plotted with open squares. The high redshift SN plotted with filled symbol is the sole for which we have full control on the data .

I can't find "open squares." Do you mean "open diamonds"?

4.3. SN 1999Q

SN 1999Q was discovered by the HZT using the CTIO 4 m Blanco Telescope, (Riess et al., 2000). It was spectroscopically confirmed to be a type Ia at redshift $z = 0.46$. The Milky Way reddening is $E(B-V) = 0.021$ mag (Schlegel et al., 1998).

J-band observations were done at 5 different epochs, the first was observed at NTT SOFI and the following epochs at Keck NIRC. Our *K*-corrections to the data disagree with the value applied to all epochs in Riess et al. (2000), with differences up to ~ 0.15 mag at late time. The restframe *I*-band computed are given in Table 7.

data

Restframe *B*-band lightcurve was not reported in the original paper. However, publicly available data at HST were used to estimate the *B*-band stretch factor. This was obtained by fixing the time of maximum to $MJD_{\max} = 51194.65$ (John Tonry, private communication). The value fitted is $s_B = 1.102 \pm 0.026$.

MJD	Epoch	I(mag)
51204.2	6.9	23.80 ± 0.15
51216.4	15.18	24.14 ± 0.18
51239.3	30.9	24.47 ± 0.15
51243.3	33.88	24.28 ± 0.15
51261.3	45.98	24.52 ± 0.20

Table 7 Summary of IR data of SN 1999Q. Epochs are in restframe relative to *B*-band maximum; restframe *I*-band magnitudes are computed applying *K*-corrections using the spectral template in (Nobili et al., 2003) to the observed *J*-band data published in Riess et al. (2000), and adding the offset found between optical and IR systems. The uncertainties also include the contribution from *K*-corrections, estimated to be 0.05 mag at all epochs considered.

4.4. Lightcurve fit of the high redshift supernovae.

The *I*-band lightcurves of the high redshift supernovae are not well sampled in time as the low redshift sample analyzed in

this work. There are only few data points for each SN, making it impossible to perform the 5 parameter fit. Thus, we used the results of the fit of the local sample of supernovae to build a set of *I*-band templates, which in turn have been used to fit the high redshift SN lightcurves.

The best fit lightcurve for each of the 42 supernovae in our low-redshift sample can be viewed as defining an *I*-band template. The high-redshift supernovae are fit to each template with a single free parameter, $I_{\max}$, the absolute normalization of the template. In all the cases we assumed the time of $B_{\max}$ to be known from the sources for the published data, and our *B*-band lightcurve fit for SN 2000fr has been performed again using the improved templates. A χ^2 comparison was used to choose the best low redshift template. In the case of SN 1999Q, the data point at day +45 was excluded from the fit for consistency, since only data up to day +40 were used to fit the low redshift lightcurves.

Figs. 9-11 show the comparison of the data with the best fit template for each of the supernovae. Table 8 gives the results of the fit together with redshift, the number of data points, the template giving the best fit and the χ^2. As there are few data points for each SN, the χ^2 parameter has little significance for estimating the goodness of the fits. Thus, to estimate the possible systematic error in the measured peak magnitude from the selection of lightcurve template, we computed the r.m.s. of the fitted I_{max} of all the lightcurve templates giving a $\chi^2 \leq \chi^2_{min} + 3$. This systematic uncertainty is reported also in Table 8. In the cases of SN 1999ff and SN 2000fr this is quite small, and compatible with the scatter due to the statistical uncertainties, thus, it is a conservative estimate. For SN 1999Q the systematic uncertainty is larger than ~~what~~ would be justified statistically. Moreover, this SN is well fitted by the template of SN 1989B, giving a similar χ^2 than the best fit one, but a fitted I_{max} about 0.2 mag brighter.

delete word: "what"

English problem: Does this mean "giving a chi2 similar to the best fit one"?

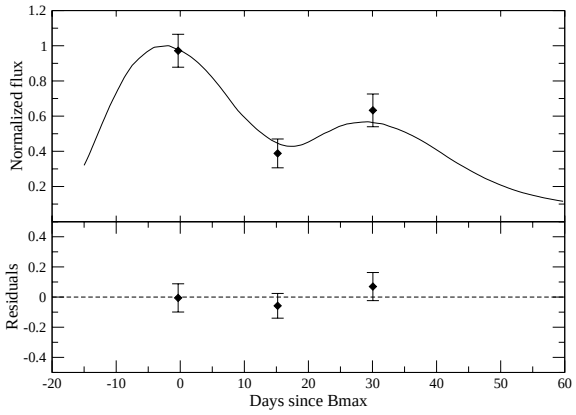

Fig. 9 *I*-band fit for SN 2000fr. Best fit was obtained with the template of the nearby SN 1992bc, out of 42 templates. The fit was performed with only one free parameter, the peak magnitude, $I_{\max} = 23.48 \pm 0.08$ mag. Supplemental data from the *B*-band (not shown) is used to fix the date of maximum.

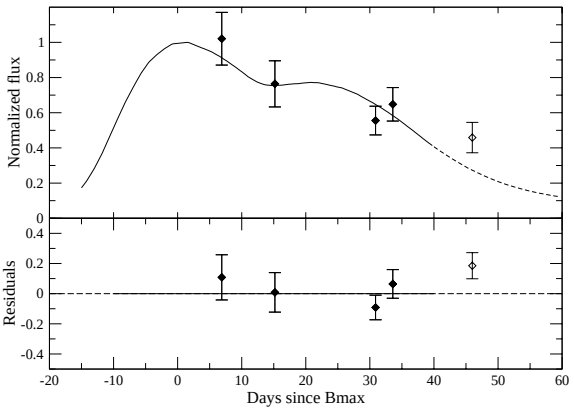

Fig. 10 *I*-band fit for SN 1999Q. Best fit was obtained with the template of SN 1999ac, out of 42 templates. The fit was performed with only one free parameter, the peak magnitude, $I_{\max} = 23.86 \pm 0.08$ mag. *B*-band date of maximum fixed to $MJD_{\max} = 51194.65$ (Tonry, private communication). The dashed line is beyond the templates definition. Thus, only data in the range of definition, plotted with closed symbols, are considered for the fit.

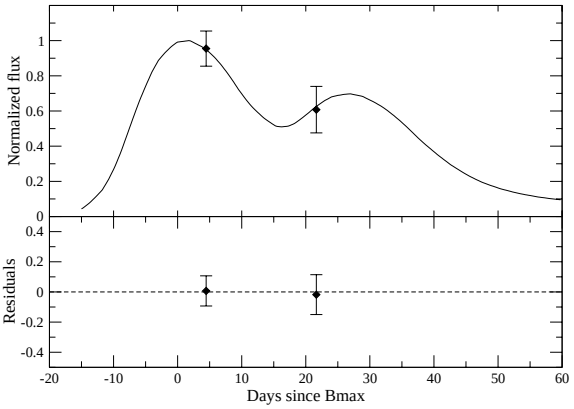

Fig. 11 *I*-band fit for SN 1999ff. Best fit was obtained with the template of SN 1999bl, out of 42 templates. The fit was performed with only one free parameter, the peak magnitude, $I_{\max} = 23.55 \pm 0.10$ mag. Supplemental data from the *B*-band (not shown) is used to fix the date of maximum.

4.5. Monte-Carlo test of the fitting method

A Monte-Carlo simulation was run in order to test the fitting method applied to the high redshift SNe. The uncertainties on the data were used to generate a set of 1000 SNe, randomly distributed around the data points, at the same epochs of the data. All the simulated data sets were in turn fitted with the 42 templates and the one giving the minimum χ^2 was selected for each simulation. The distribution of the maximum peak fitted in each of the simulated data sets around the value fitted on the experimental data was studied to check for systematic uncertainty in the fitting procedure. This was found to be robust, always selecting the same template as the one giving the best fit for all the three SNe. No bias was found, therefore confirming the peak magnitude fitted with this method. The uncertainty on

The first paragraph of this section 5 should probably be slightly reworded, since it seems to imply that we only did Milky Way extinction correction *because* we wanted to plot a Hubble diagram!

SN	z	s_B	n	$I_{\max}$	template	χ^2	A_J^{MW}
SN 2000fr	0.543	1.034 ± 0.011	3	23.48 ± 0.08 ± 0.04	SN 1992bc	1.04	0.027
SN 1999ff	0.455	0.80 ± 0.05	2	23.55 ± 0.10 ± 0.08	SN 1996bl	0.05	0.022
SN 1999Q	0.460	1.102 ± 0.026	4	23.86 ± 0.08 ± 0.14	SN 1999ac	2.12	0.019

Table 8 List of the high redshift type Ia SNe used in this work. Columns are: redshift, number of data points used in the fit, magnitude of the peak resulted from the fit (both statistical and systematic uncertainties are given), best fit template, χ^2 of the fit, Milky Way extinction in the J-band.

It's not clear here (or in the text) if this I_max value is before or after correctinf for Milky Way extinction.

Insert the word "here" instead of "of this work", since otherwise it implies this is the only goal of the paper.

$I_{\max}$ reported in Table 8 was consistent with the dispersion in the distribution measured on the simulations.

three

5. The I-band Hubble diagram up to $z \sim 0.5$

The goal ~~of this work~~ is to add the three high redshift SNe in the Hubble diagram. The I-band peak magnitudes of the high redshift supernovae, reported in Table 8, were ~~thas~~ corrected for Milky Way extinction. Note that all ~~the~~ SNe have been reported not to suffer from extinction in the host galaxy.

The Hubble diagram has been built both without and with width-luminosity correction (case a and case c respectively), were the systematic uncertainties on the peak magnitudes of the distant supernovae, listed in Table 8, are added in quadrature to the statistical uncertainties. Cases b and d are like a and c but neglecting the systematic uncertainties in Table 8. Figure 12 shows the extended Hubble diagram (case c), where an intrinsic uncertainty of 0.13 mag has been added in quadrature to the measurement errors of the plotted data. The solid line represent the best fit to the nearby data for the concordance model $\Omega_M = 0.3$ and $\Omega_\Lambda = 0.7$. Also plotted is the model for $\Omega_M = 1$ and $\Omega_\Lambda = 0$ (dashed line), and a flat, $\Lambda = 0$ universe in presence of a homogeneus population of large grain dust in the intergalactic (IG) medium able to explain the observed dimming of type Ia SNe at $z \sim 0.5$ in the B-band (dotted line) (Aguirre, 1999a,b). The bottom panel shows the residuals obtained for case a. Table 9 lists the χ^2 values for the high redshift SNe to each of the model. The concordance model results are consistent with the data. The low statistics of the high redshift sample is insufficient to draw strong conclusions on cosmological parameters.

[This is one of the places where it is not clear why Omega_m=0.25, Omega_Lambda=0.75 wasn't used.]

$(\Omega_M, \Omega_\Lambda)$	χ^2_a	χ^2_b	χ^2_c	χ^2_d
(0.3,0.7)	2.09	2.90	4.62	10.21
(1,0)	6.08	8.31	14.40	26.94
$(1,0)_{dust}$	3.43	4.82	8.09	16.54

Table 9 Reduced χ^2 (for 3 *dof*) of the high redshift data to each model, without stretch correction and with systematic uncertainties added in quadrature (χ^2_a), neglecting the systematic uncertainties (χ^2_b), with stretch correction and adding the systematic uncertainties in quadrature (χ^2_c) or neglecting them (χ^2_d).

The scatter between the z~0.5 points is 0.34 ± 0.07 mag, i.e. slightly too large to be consistent with the quoted measurement errors. In this sense, and also given the very limited statistics available, additional unidentified systematic uncertainties on the distant SNe cannot be excluded.

A general problem concerns J-band observations, that correspond to the restframe I-band at the redshift considered. Infrared data reduction and calibration, involving conditions rapidly evolving with time, remain more problematic ~~to what~~ is the case at optical wavelengths. In this sense, infrared observations from space are desirable.

"than"

Some uncertainties are specific to the sample considered here. The different fitting methods applied to the restframe I-band lightcurve for the low and high redshift samples can be easily overcome if distant supernovae are followed at NIR wavelengths with better time coverage. Both the low and high redshift samples used in this analysis are rather heterogeneous, as they were collected from different data sets. Future data sets collected with a single instrument would naturally solve this problem.

6. SN colors and study of gray dust

Multi-color photometry allows for extinction tests for non-standard dust with only weak wavelength dependence, such as the reddening by a homogeneous population of large grain dust, as proposed by Aguirre (1999a,b). Assuming a density of gray dust in the IG medium to explain the observed dimming of supernovae at redshift $z = 0.5$ in B-band with $\Omega_M = 1$ and $\Omega_\Lambda = 0$, we calculated the expected color extinction following Goobar et al. (2002a) using the SNOC Monte-Carlo package (Goobar et al., 2002b), for two cases of $R_V = 4.5$ and $R_V = 9.5$ and a comoving dust density between z=0 and the SN redshifts.

For two of the three SNe considered in this work we computed rest frame $B - V$ and $B - I$. For the third supernova, SN 1999Q, only $B - I$ is available. Table 10 and 11 lists the colors for all the SNe, corrected for Milky Way extinction. The color evolution has been compared to models for a Λ dominated universe and a $\Omega_M = 1$, $\Omega_\Lambda = 0$ universe with presence of gray dust (R_V=4.5 and R_V=9.5) accounting for the faintness of type Ia supernovae at $z \simeq 0.5$, and it is shown in Figure 13. The error bars include also the intrinsic color dispersion contribution.

The χ^2 has been computed for both $B - V$ and $B - I$ evolution for each supernova and for all the supernovae together (see Table 12). The correlations between SN colors at different epochs found in (Nobili et al., 2003) were taken into account. However, we note that, although this correlation should be taken into account in the calculations, neglecting it would not change significantly the conclusions of the analysis. Although individual supernovae give χ^2 values that would seem to distinguish between the models being compared, the combination of the three SNe disfavour such conclusions. For instance, Riess

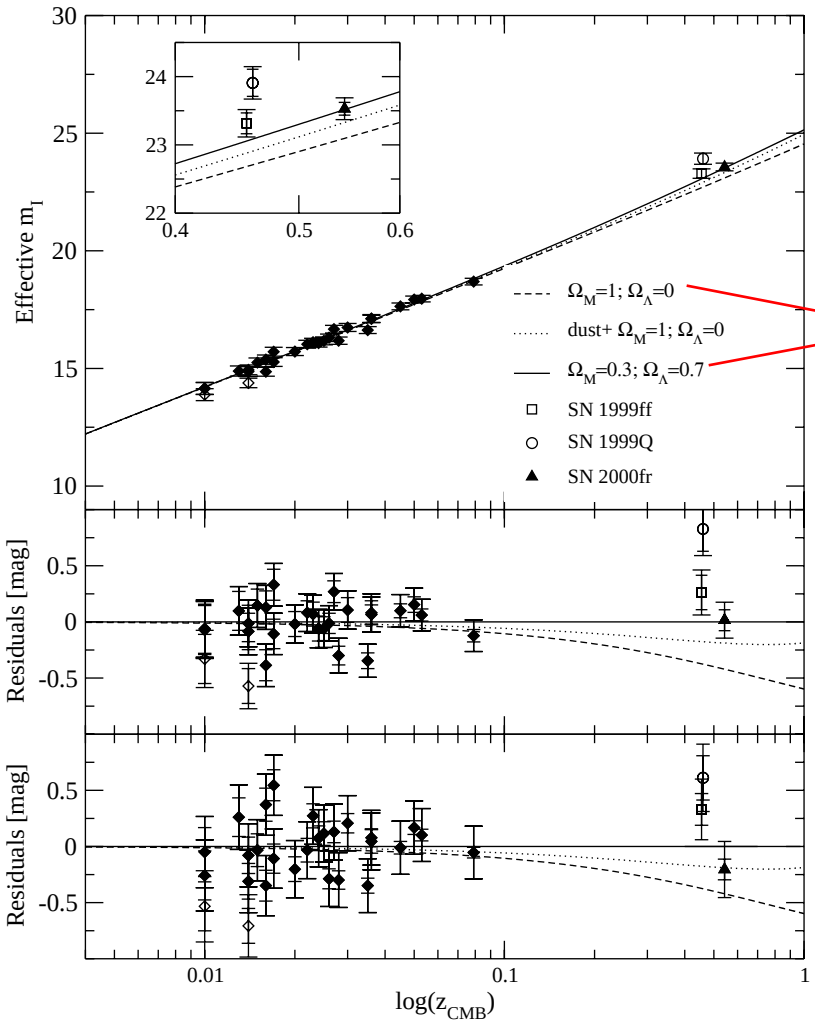

Switch these labes so they appear in the same order as the sequence of lines on the plots.

Fig. 12 Effective *I*-band maximum vs redshift for the nearby supernovae of the Calan/Tololo, CfA and CfA2 sample, together with three supernovae at redshift $\sim$ 0.5 for case *c* (top panel), residuals to the $(\Omega_M, \Omega_\Lambda)$=(0.3,0.7) model for case *c* (middle panel) and case *a* (bottom panel). SN 1998es and SN 1999dq were excluded from the fit (see text) and are plotted with open diamonds. The high redshift SNe plotted with open symbols are the ones for which the photometry has been taken from literature, and the *K*-corrections have been applied by the authors using the improved spectral template (see text for details).

et al. (2000) used the $B-I$ color of SN 1999Q to rule out the gray dust hypothesis. However, when combined with the other two supernovae in this analysis, SN 1999ff in particular, for which we also have used $B-V$ color, no such conclusion may be drawn.

To make our test for gray dust more robust a different approach was followed. The method of least squares has been used to combine color measurements along time for each supernova (see Cowan, 1998, p.106 for details) ~~for details.~~ The residuals of each supernova colors to the expected model, plotted in Figure 13, are weighted averaged together, and the covariance matrix is used as weight in the calculation. In the following, we refer to $E(X-Y)$, to describe the color excess of any supernova with respect to the $X-Y$ average color of local supernovae, as derived in (Nobili et al., 2003). First we applied this method to all local supernovae and used the results to establish the expected distribution in the $E(B-I)$ vs $E(B-V)$ plane, as showed in Figure 14.

delete>

As the high redshift SNe were not corrected for host galaxy extinction, we computed the local sample distribution for two cases: the left panels represent the distribution of color excess of 27 nearby SNe not corrected (top panel) and corrected (bottom panel) for host galaxy extinction, where the spectroscopic peculiar SNe have been excluded from the analysis. The size of the ellipses on each color axis is given by the estimated one-dimensional standard deviation of the distribution and the inclination is defined by the linear Pearson correlation coefficient computed on the same data sample. The solid contours represent 68.3%, 95.5% and 99.7% probability.

The right panels in Figure 14 show the combined values of color excess for the high redshift supernovae, where SN 1999Q is represented by a band (horizontal dashed-lines), as the $B-V$ color is missing. These are compared to the local supernova

These two highlighted phrases seem to contradict each other: is it 1-D standard deviation, or is it 68%, 95%,... which seems to suggest a 2-D included probability region.

day	$B-I$
SN 2000fr	
-0.32	-0.51 ± 0.12
14.70	-0.50 ± 0.24
29.08	1.42 ± 0.17
SN 1999ff	
5.59	-0.18 ± 0.13
27.20	1.38 ± 0.24
SN 1999Q	
6.25	-0.57 ± 0.15
13.78	-0.04 ± 0.18
28.03	1.21 ± 0.15
30.48	1.57 ± 0.15
41.73	1.76 ± 0.20

Table 10 Restframe $B-I$ colors in magnitudes for the three high redshift SNe. Time is divided by the B-band stretch.

day	$B-V$
SN 2000fr	
-7.97	-0.06 ± 0.05[a]
-3.51	-0.14 ± 0.05[a]
4.60	-0.12 ± 0.05
12.93	0.24 ± 0.08
20.31	0.61 ± 0.07
30.22	0.99 ± 0.09
SN 1999ff	
-7.99	0.03 ± 0.08[a]
1.91	-0.02 ± 0.09
1.98	0.10 ± 0.12
2.91	0.23 ± 0.12
19.55	0.71 ± 0.09
28.75	1.22 ± 0.20

Table 11 Restframe $B-V$ colors in magnitudes for the two of the high redshift SNe. Time is divided by the B-band stretch.

[a]data not included in the analysis because out of the range in which Nobili et al. (2003) studies color correlations.

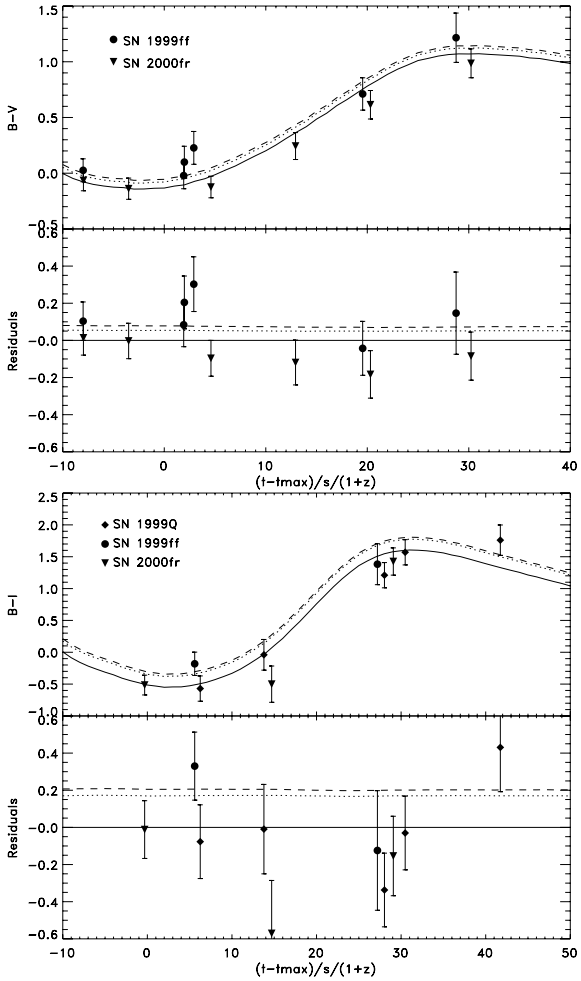

Fig. 13 High redshift SNe color evolution, $B-V$ (top panel) and $B-I$ (bottom panel), compared to a Λ dominated universe (solid line) and to an $\Omega_M = 1$, $\Omega_\Lambda = 0$ universe with presence of gray dust with R_V=4.5 (dashed line) and R_V=9.5 (dotted line). **Symbols for 99Q and 99ff will be soon changed in open symbols as in figure 12**

distribution (dotted lines), that represent the distribution expected in the absence of IG dust. Also plotted is the 68.3% level of the expected distribution in presence of "gray" dust with $R_V = 9.5$, represented by the ellipse (dashed line) displaced by (0.06,0.19) from the no-dust model. Only the case of $R_V = 9.5$ has been plotted for readability reasons, given the small difference between the two dust models. Note that this is the model closer to no-dust model. The ellipse corresponding to $R_V = 4.5$ would be displaced by (0.03,0.04), respectively in $E(B-V)$ and $E(B-I)$, from the latter.

We computed the χ^2 of the high redshift data for each model (with and without IG dust), for both the situation in the top and bottom panels of Figure 14. For each model, we sum the χ^2 contribution from all SNe. In particular, for SN 1999ff and SN 2000fr we take into account the correlation found between $E(B-V)$ and $E(B-I)$ in the nearby sample. The reduced χ^2 (for 5 degrees of freedom) are 0.70, 1.89 and 1.55 for the no-dust, IG dust with $R_V = 4.5$ and IG dust with $R_V = 9.5$ model respectively, for the host-galaxy extinction corrected case, and 0.98, 2.53 and 2.18 uncorrected. According to these results, presence of IG dust with $R_V = 4.5$ is disfavoured at 90% C.L. and at 97% C.L. in the two cases respectively, while, less stringent limits are found for IG dust with $R_V = 9.5$. However, the statistical significance of these results is very limited, and should only be taken as an example of the method developed here.

A Monte Carlo simulation was used to estimate the minimum sample size needed to test for presence of homogeneously distributed gray dust in the IGM. SNe colors were generated following the binormal distribution defined by the SN local sample. Under the assumption that the systematic effects are negligible and an average measurement uncertainty of 0.05 mag in both $E(B-V)$ and $E(B-I)$, we found that a sample of at least 20 SNe would be needed to be able to exclude the dust models at the 95% C.L.

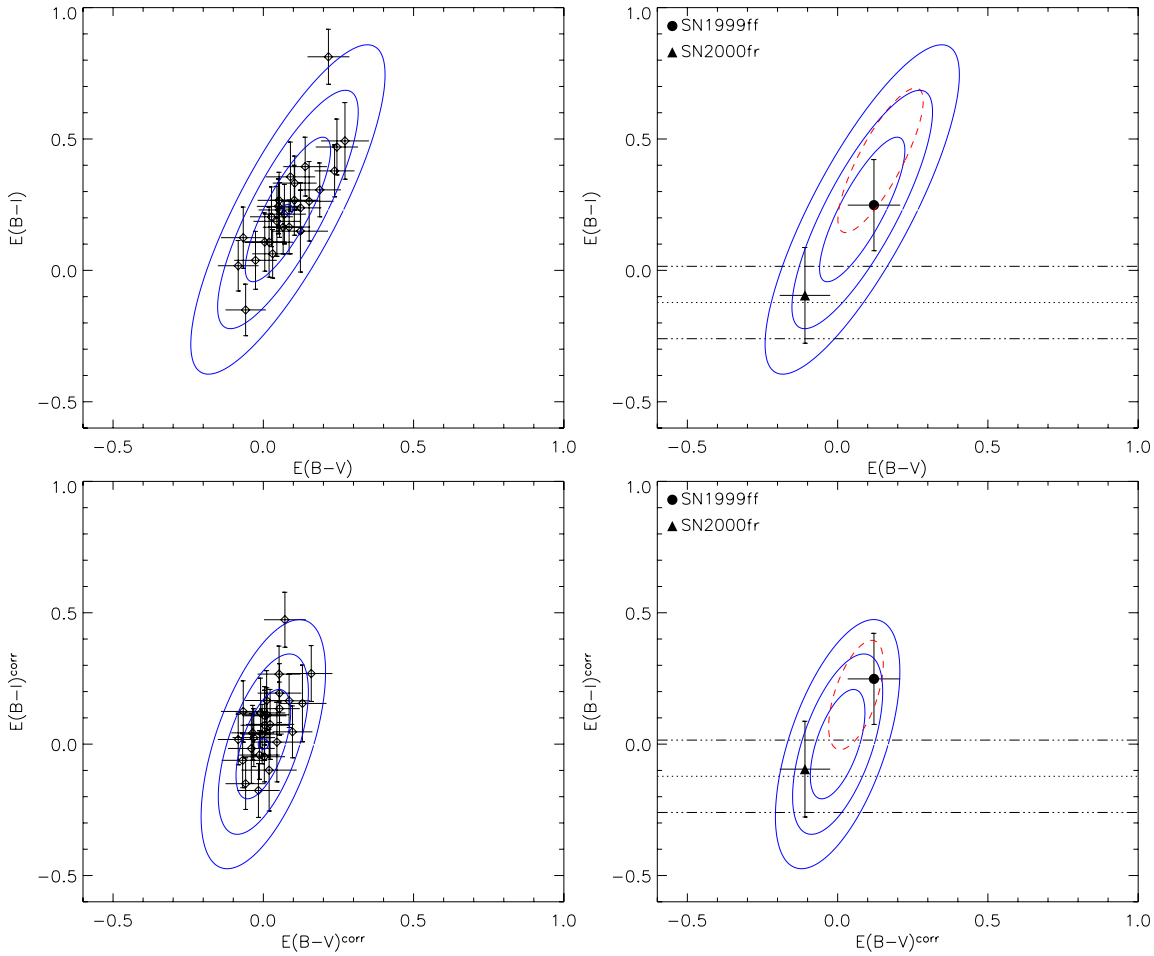

Fig. 14 Left panels: distribution of combined color measurements for the local sample of supernovae in the $E(B-I)$ vs $E(B-V)$ plane, not corrected (top panel) and corrected (bottom panel) for the host galaxy extinction. The solid contour is 68.3%, 95.5% and 99.7% of probability. Right panels: combined colors of the high redshift supernovae compared to the distribution in the absence of IG dust (solid ellipses), and the one expected in presence of gray dust in the IG medium with $R_V = 9.5$ (dashed ellipse). SN 1999Q is represented by an horizontal dashed-dotted line band, as the $B-V$ color is missing, SN 1999ff by the filled circle and SN 2000fr by the filled triangle. For simplicity only the 68.3% level has been plotted for the dust distribution. **Symbols for 99ff will be soon changed in open symbols as in figure 12**

However, the possibility for the result to be affected by systematic effects is not negligible. Increasing the sample and the time sampling for each object would allow us not only to improve the significance of our statistic, but it will also be a means to identify and quantify systematic effects involved.

7. Test for SN brightness evolution

Evolution of the properties of the supernova progenitors with redshift has been often proposed as an alternative explanation to the observed dimming of distant SNe. This is based on the fact that older galaxies show different composition distribution than younger ones, e.g. an increased average metallicity, therefore offering different environmental conditions to the exploding star. A simple way to test for evolution is to compare properties of nearby SNe with distant ones. This will not prove that there is no evolution, but it will exclude it on a supernova-by-supernova or property-by-property basis, finding always counterparts of distant events in the local sample.

In this work we compared colors of nearby and distant supernovae (primarily to test presence of "gray" dust). Although the size of the high redshift sample is very limited, our attempt does not give evidence for evolution of the average SN colors. Furthermore, the correlation found between the intensity of the secondary peak of I-band lightcurve and the supernova luminosity give an independent way of testing for evolution. The restframe I-band lightcurve for the high-redshift supernovae were all fitted by templates showing a prominent second peak, i.e. inconsistent with the intrinsically underluminous supernovae necessary to explain the apparent faintness of high redshift supernovae in a flat $\Lambda = 0$ universe. Note that, for at least one supernova, SN 2000fr, the secondary peak is evident on the data even prior to the lightcurve fit. Table 13 lists the $\Delta\chi^2$ for the fit of the high redshift SNe to the templates of the two sub-luminous SN 1991bg and SN 1997cn, relative to the

We should emphasize that this is a new contribution of this paper by changing this sentence to some thing like:
"Note that the data presented here for SN 2000fr shows for the first time a case where the secondary peak is evident in the data even prior to the lightcurve fit."

	χ^2_{B-V}/dof	χ^2_{B-I}/dof
SN 2000fr		
no dust, $(\Omega_M, \Omega_\Lambda)$=(0.3,0.7)	2.33/4	2.08/3
dust R_v = 9.5, $(\Omega_M, \Omega_\Lambda)$=(1,0)	4.24/4	3.94/3
dust R_v = 4.5, $(\Omega_M, \Omega_\Lambda)$=(1,0)	5.29/4	4.50/3
SN 1999ff		
no dust , $(\Omega_M, \Omega_\Lambda)$=(0.3,0.7)	6.05/5	3.93/2
dust R_v = 9.5, $(\Omega_M, \Omega_\Lambda)$=(1,0)	4.69/5	2.06/2
dust R_v = 4.5, $(\Omega_M, \Omega_\Lambda)$=(1,0)	4.31/5	1.89/2
SN 1999Q		
no dust, $(\Omega_M, \Omega_\Lambda)$=(0.3,0.7)	—	3.36/4
dust R_v = 9.5, $(\Omega_M, \Omega_\Lambda)$=(1,0)	—	7.06/4
dust R_v = 4.5, $(\Omega_M, \Omega_\Lambda)$=(1,0)	—	8.10/4
All the SNe combined		
no dust , $(\Omega_M, \Omega_\Lambda)$=(0.3,0.7)	8.38/9	9.36/9
dust R_v = 9.5, $(\Omega_M, \Omega_\Lambda)$=(1,0)	8.93/9	14.49/9
dust R_v = 4.5, $(\Omega_M, \Omega_\Lambda)$=(1,0)	9.59/9	13.05/9

Table 12 χ^2 computed for the 3 different models and colors for each of the supernovae and for all of them combined.

	n	SN 1991bg	SN 1997cn
SN 2000fr	3	24.03	21.73
SN 1999ff	2	3.28	2.72
SN 1999Q	4	21.25	27.38

Table 13 $\Delta\chi^2$ for the fit of the high redshift SNe to the templates of the two sub-luminous SNe relative to the best fits (which are "normal" SN templates). n is the number of data points used in the one-parameter fit (see discussion in section 4.4).

best fit. The χ^2 values are significantly larger than the best fit value.

8. Summary and conclusions

In this work we have investigated the feasibility of using restframe *I*-band observations for cosmological purposes.

We have developed a five parameter lightcurve fitting procedure which was applied successfully to 42 nearby type Ia supernovae. The fitted lightcurve were used to build a set of templates which include a broad variety of shapes. We have found correlations between the fitted parameters, in particular between the time of the secondary peak and the *B*-band stretch, s_B. Moreover, a width-luminosity relation was found for the *I*-band peak magnitude both with s_B and with the *I*-band stretch, s_I.

We built a restframe *I*-band Hubble diagram using 26 nearby supernovae at redshifts $0.01 \leq z \leq 0.1$, and measured an r.m.s. of 0.24 mag, smaller than the uncorrected dispersion corresponding to restframe *B*-band. The width-luminosity relation was used to reduce the r.m.s. to 0.17 ± 0.03 mag, corresponding to an intrisic dispersion of 0.13 mag. Differences between the three data samples are also discussed.

J-band measurements of three high redshift supernovae were used to extend the Hubble diagram up to $z \sim 0.5$. Their restframe *I*-band lightcurve was fitted by the template set built on the local SNe sample, as the five parameter fit method could not be used for the poorly sampled high redshift lightcurve. The peak *I*-band magnitude of the high redshift SNe was compared to three different set of cosmological parameters. Although the "concordance model" of the universe, $(\Omega_M, \Omega_\Lambda)$=(0.3,0.7), is found in better agreement with the data than the other models, the large dispersion of the high redshift supernovae, together with the low statistics of the sample, do not allow to reach firm conclusions.

Alternative explanations of the observed dimming of supernova brightness, such as presence of gray dust in the IG medium or evolution effects in the supernova properties have also been addressed. Both the *I*-band Hubble diagram and multi color photometry have been used for testing gray dust. Although no firm limits on the presence of gray dust could be set, this study shows that with higher stastistics, the restframe *I*-band measurements could provide useful information on cosmological parameters, including tests for systematic effects. A Monte Carlo simulation indicates that a sample of at least 20 well observed SNe would be enough for testing the presence of a homogeneous dust distribution in the IGM, using only the color diagram technique. A similar technique, but using QSO colors was used by Mörtsell & Goobar (2003), to rule out gray dust being the sole explanation for the apparent faintness of SNe Ia at $z \sim 0.5$.

Possible systematic uncertainties affecting the restframe *I*-band Hubble diagram are discussed. Some sources are identified, for instance the different methods applied for fitting the low and the high redshift samples, selection effects for bright objects during the search campaign, uncertainties connected with the *J*-band data calibration, as well as uncertainties in the *K*-correction calculations due to the presence of the Ca IR triplet feature in the near infrared region of the SN spectra. However, these systematic uncertainties differ from the ones that could affect the restframe *B*-band Hubble diagram. Thus,the use of *I*-band measurements of type Ia supernovae, can be complementary to the already well established tools.

Acknowledgements. S.N. is supported by a graduate student grant from the Swedish Research Council.

"sets"

Add telescopes/observatories acknowledgements and LBNL funding acknowledgements (and other funding?) -- get these all from Tony.

References

,Aldering, G.,2000, coex.conf, 75A
Aguirre, A. 1999, ApJ, 512, L19
Aguirre, A. 1999, ApJ, 525, 583
Balbi, A., Ade, P., Bock, J. et al., 2000, ApJ, 545, L1.
Bessell, M.S., Castelli, F. & Plez, B. 1998, A&A, 333, 231
Borgani, S., Rosati, P., Tozzi, P. et al. 2001, ApJ, 561, 13
Cardelli, J. A, Clayton, G.C. & Mathis, J.S.1989, ApJ, 345, 245
Carpenter, J.M., 2001, AJ, 121, 2851C
Cohen, M., Wheaton, WM. A. & Megeath, AJ, 2003, 126,1090
Contardo, G., Leibundgut, B. & Vacca, W. D. 2000, A&A , 359, 876C
Cowan, G., 1998, Statistical data analysis, Oxford University Press
C. Csaki, N. Kaloper & J. Terning, hep-ph/0111311.
De Bernardis, P., Ade, P.A.R., Bock, J.J. et al., 2000, Nature, 404,955

Delete stray comma.

C. Deffayet, D. Harari, J. P. Uzan & M. Zaldarriaga, hep-ph/0112118.
Drell, P., Loredo, T.& Wasserman, I., 2000, ApJ, 530, 593.
Efstathiou, G., Moody, S., Peacock, J.A. et al, 2002, MNRAS, 330, L29.
Filippenko, A.V., Richmond, M.W., Branch, D. et al., 1992, AJ,104,1543
Garavini, G. et al. 2004 (in prep)
Garnavich, P.M., Jha, S., Challis, P., 1998,ApJ, 509, 74
Goldhaber, G., Groom, D. E.,Kim, A. et al.,2001, ApJ, 558, 359G
Goobar, A., Bergström, L. & Mörtsell, E., 2002, A&A, 384, 1.
Goobar, A., Mörtsell, E., Amanullah, R., Goliath, M., Bergström, L. & T. Dahlen, 2002, A&A, 392, 757.
Hamuy, M., Maza, J., Wischnjewsky, M. et al. 1993, IAUC, 5723R
Hamuy, M., Phillips, M.M., Suntzeff, N.B. et al. 1996, AJ, 112, 2408
Hamuy, M., Phillips, M.M., Suntzeff, N.B. et al. 1996, AJ, 112, 2398H
Henry J. P. 2001, ApJ 534, 565
Howell, D.A, 2001, ApJ,554, 193
Jaffe, A.H., Ade, P.A., Balbi, A. et al., 2001, Phys. Rev. Lett. 86, 3475
Jha, S., 2002, PhD thesis, Harvard University.
Kim, A., Goobar, A. & Perlmutter, S., 1996, PASP, 108, 190
Knop, R. et al. 2003, submitted
Krisciunas, K., Phillips, M.M., Stubbs, C. et al., 2001, AJ, 122, 1616K
Krisciunas, K., Phillips, M. M. & Suntzeff, N. B., astro-ph/0312626
Leibundgut, B., Kirshner, R. P., Phillips, M.M. et al., 1993,AJ, 105, 301.
Li, W., Filippenko, A.V. & Treffers, R.R., 2001, ApJ, 546,734
Lidman, C. et al. 2004 (in prep)
Maza, J., Hamuy, M., Phillips, M., Suntzeff, N. & Aviles, R., 1994, ApJ,424,L107
Mörtsell, E., Bergström, L and Goobar, A., 2002, Phys. Rev. D66, 047702.
Mörtsell, E. & Goobar, A., 2003, JCAP, 09, 009M
Nobili, S., Goobar, A., Knop, R., & Nugent, P., 2003, A&A 404, 901-912
Nugent, P. & Aldering, G., 2000, sgrb.conf, 47N
Nugent P., Kim A.& Perlmutter S., 2003, PASP 114, 803
Perlmutter, S., Gabi, S., Goldhaber, G., 1997,ApJ, 483, 565
Perlmutter, S., Aldering, G., Goldhaber, G. et al., 1999, ApJ, 517, 565
Persson, S.E., Murphy, D.C., Krzeminski, W., Roth, M. & Rieke, M.J., 1998 A.J. 116, 2475.
Phillips, M.M., Lira, P., Suntzeff, N.B., Schommer, R.A., Hamuy, M.& Maza, J., 1999, AJ, 118:1766-1776
Richmond, M.W., Treffers, R.R., Filippenko, A.V. et al. 1995, AJ 109,2121
Riess, A., et al. 1998, AJ, 116, 1009.
Riess, A.G., Filippenko, A.V., Challis, P. et al. 1999, ApJ. 117,707-724
Riess, A.G., Filippenko, A.V., Liu, M.C. et al., 2000, ApJ. 536,62-67
Rowan-Robinson, M.,2002,MNRAS, 332, 352.
Schlegel, D.J., Finkbeiner, D.P. & Davis, M. 1998, ApJ, 500, 525S
Schuecker, P. Böhringer, H., Collins, C. A. & Guzzo, L., 2003, A&A, 398, 867
Sievers, J.L., Bond, J.R., Cartwright, J.K. et al., 2003, ApJ.,591, 599
Spergel, D.N., Verde, L., Peiris, H.V. et al., 2003, ApJS, 148, 175S
Tonry, J.L.,Schmidt B.P., Barris, B. et al 2003,astro-ph/0305008
Wang, L., Goldhaber, G., Aldering, G., Perlmutter, S.2003, ApJ, 590, 944
Wang, L., 2003, Submitted to ApJL
Wells, L.A., Phillips, M.M., Suntzeff, B. et al., 1994 AJ 108, 2233